Damage Tolerance Assessment of Naval Sandwich Structures with Face-Core Debonds

Christian Berggreen and Brian Hayman

1 Introduction

Sandwich structures offer superior stiffness/weight and strength/weight ratios compared with monolithic composites and traditional metallic structural concepts, and are thus of great interest for lightweight structural applications in naval ships. For marine applications, the sandwich face sheets have traditionally been made of glass fibre reinforced polymer (GFRP), the matrix being polyester, vinylester or epoxy, while the core has been either balsa wood or a polymer foam such as polyvinyl chloride (PVC). More recently carbon fibre reinforcement has also been introduced, while for naval ships the use of balsa cores has been limited to some superstructure components and internal structures.

Such sandwich structures contain imperfections resulting from either the production processes or subsequent handling and use. Many fibre reinforced polymer (FRP) structures have traditionally been designed without explicitly addressing such defects and damage; production defects have been allowed for by applying high factors of safety, and a certain degree of robustness in relation to accidental events has been built-in by such means as the minimum thickness or minimum reinforcement requirements in classification society rules.

In contrast, the aircraft industry has focused more explicitly on defects and damage by requiring fail-safe or damage tolerant design. As more optimised, lightweight composite designs have become established in marine applications, particularly for naval and high-speed vessels, the need for adopting damage tolerance principles in these applications has become evident. However, because the operating conditions, in-service inspection regimes and safety considerations differ

C. Berggreen (✉) · B. Hayman
Department of Mechanical Engineering, Technical University of Denmark, Kongens Lyngby, Denmark
e-mail: cbe@mek.dtu.dk; bhayman@mek.dtu.dk

from those for aircraft, there must be differences in the way a damage tolerance approach is implemented.

A start towards establishing a consistent damage tolerance approach for naval sandwich structures was made several years ago in the project THALES JP3.23: Inspection and Repair of Sandwich Structures in Naval Ships (SaNDI), a collaboration between the Norwegian, Swedish, Danish, Finnish and British navies, research institutions, shipyards and other suppliers of materials and services [1]. Attention was focused on the types of defects and damage that need to be taken into account when naval ships built in FRP sandwich are designed, built, maintained and operated, on the methods available to detect such defects and damage, on the ways in which their influence on structural performance may be assessed, and on the methods available for their repair. The project developed an integrated methodology [2–4] for the inspection, assessment and repair of defects and damage, with attention to the important questions of whether, when, where and how defects and damage should be repaired and, in the case of in-service damage, whether measures should be taken to impose operational restrictions in the interim period while a repair is pending. An overview of some of the main results was presented by Hayman [5], together with discussion of the implications for introducing more damage tolerant design in FRP structures in ships and other applications.

The terms "defect" and "damage" are not uniquely defined for all contexts, and are sometimes used synonymously. To make a major distinction that is relevant in practice, it is convenient to use the terms "production defect" and "in-service damage". In all FRP composite structures it is important to be able to detect and rectify both production defects and in-service damage. For single-skin (monolithic) laminates and face laminates of sandwich structures, production defects include dry zones, voids, delaminations, wrinkles, misalignment of fibres, and poor curing (giving reduced physical properties). For sandwich structures, the following types of production defects must also be considered: face-core debonds, voids and inclusions in the core, and lack of bond (edge-to-edge and face-to-face) between core sheets. In aircraft structures the main type of in-service damage is impact damage, typically from bird strikes, hail and objects thrown up from the runway during landing and takeoff. Ship structures, however, may encounter a wider range of contact damage (quasi-static contact, e.g. during berthing, as well as impact), incidences of heat damage, and numerous types of damage resulting from overloading. This last category includes core fracture or crushing, face-core debonds, laminate rupture, delamination either within a laminate or at a joint made by secondary lamination, and failure at equipment fastenings. Impact damage may be confined to the impacted face laminate (with or without penetration of the laminate), or may involve crushing and/or cracking of the core. In extreme cases, penetration of the entire sandwich may occur. More substantial damage cases include the removal of whole panels or assemblies by fire or collision. For naval vessels some types of damage may be caused by weapon effects such as air blast, underwater explosions, and fragment or missile hits.

A common type of defect or damage that can seriously affect the integrity of a sandwich structure is a lack of adhesion between the face sheets and the core commonly known as a "debond" (or typically as a "disbond" in the aerospace industries). In connection with the SaNDI project, Berggreen [6], in a doctoral thesis at the Technical University of Denmark (DTU), studied the damage tolerance of debonded sandwich structures and initiated a long series of major contributions to this field of research. Several years previously Zenkert had also considered the problem of face-core debonds [7] in connection with his own doctoral thesis [8] at the Royal Institute of Technology (KTH) in Sweden that concerned damage tolerance of foam-cored sandwich structures. At about the same time, with support of the US Office of Naval Research (ONR), Carlsson and co-workers were also studying the fracture characterisation of face-core interfaces and the effect of debonds on the in-plane compressive strength of sandwich columns and panels. In subsequent years, immense progress has been made in this area in both Europe and the USA, much of the work being supported by the ONR, but with some close links also being established in recent years with the aircraft industry and also the wind turbine industry, where sandwich components with material configurations similar to those in marine vessels are applied in large quantities. In particular, while the SaNDI project and many other earlier studies were limited to the effects of defects and damage on static strength, recent studies of sandwich debonds have increasingly focused on debond crack propagation under fatigue loadings.

To provide a coherent, damage tolerance-based approach to sandwich structures each of the following aspects must be addressed:

- Understanding of the fracture mechanics of sandwich debonds, including especially the effects of mode mixity, i.e. combinations of the fracture modes I and II (and possibly III).
- Establishment of experimental techniques to determine the interface properties for the respective fracture modes and degrees of mode mixity.
- Development of methods of modelling crack propagation under increasing load and under repeated (fatigue) loading
- Experimental studies, and the use of experiments to validate modelling techniques, both at the level of simple sandwich beam specimens used for material characterisation and at the level of structural components such as sandwich panels.
- Development of practical ways of implementing results in damage assessment schemes.

These aspects are addressed in the following sections. While the main focus is on recent research at DTU and collaborating organisations that has been supported by the ONR, some earlier research that provided a basis for this more recent work is also outlined. Note that some of these topics are addressed in Chap. 12 of the textbook by Carlsson and Kardomateas [9].

2   Fracture Mechanics of Sandwich Face/Core Interfaces

2.1   Griffith Criterion and Use of LEFM

Analysis of the development and propagation of face-core debonds in sandwich structures requires the use of fracture mechanics principles taking account of the difference in properties between the face sheet and core materials.

In sandwich beams and panels with thin face sheets the main stress conditions of relevance in structural design are the following:

- In-plane tension, compression and shear stresses in the face sheets. Compressive and shear stresses may lead to local buckling of the face sheets, which in turn may encourage debonding.
- Transverse (out-of-plane) shear stresses, predominantly in the core. The complementary shear stresses at the face-core interface lead to mode II deformation conditions for potential debonds (Fig. 1).
- Local out-of-plane stresses generated especially at joints and equipment fixings; these can involve significant peel stresses at the face-core interface, giving predominantly mode I deformation conditions (Fig. 1).

In virtually all these cases there is some degree of mode mixity combining mode I and mode II deformations. Furthermore, in a three-dimensional sandwich panel mode III may also be present (Fig. 1).

Much research effort has been focused on

- establishing the extent to which simple tests intended to provide pure mode I or mode II data in fact are influenced by the presence of mode mixity, and how the mode mixity varies as the crack length increases during a test;
- clarifying how an interface crack actually propagates, i.e. within an adhesive layer, on the face sheet side or on the core side, and whether a crack kinks away from the interface, into the face sheet or the core;
- devising and optimising test methods that provide as closely as possible desired pure or mixed mode data;
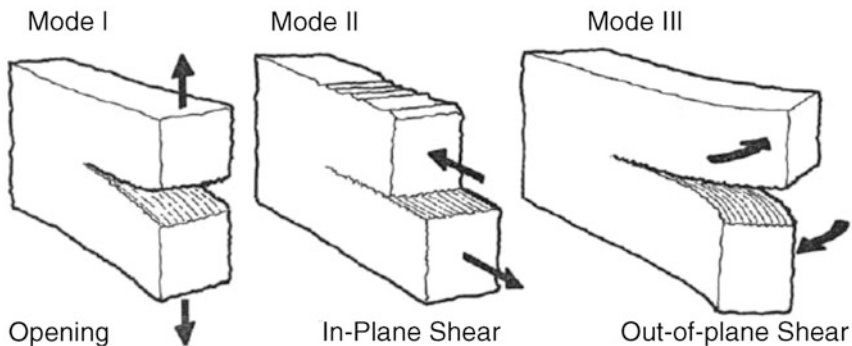

Fig. 1 The basic fracture modes

- adapting test methods originally designed for static conditions to follow crack growth under fatigue loading;
- adapting test methods to accommodate high and low temperature testing.

In the analysis of the stress state in the neighbourhood of a face-core interface, special challenges arise from the greatly differing stiffnesses between the face sheet and core materials.

For many problems in debond crack propagation inelastic deformation is confined to a very small fracture process zone, and linear elastic fracture mechanics (LEFM) can be used. The starting point for LEFM is the Griffith criterion [10], which states that a crack will propagate if the available energy release rate, G (i.e. the energy dissipated during fracture per unit of newly created fracture surface area), is greater than or equal to the fracture toughness, G_c, which is a material property that must be obtained experimentally. The fracture toughness has different values for the three main fracture modes (Fig. 1). For mixed mode fracture, at any stage in the crack propagation the strain energy release rate G and the mode mixity must first be established from analysis of the stress state in the neighbourhood of the crack, and the value of G_c for that mode mixity used in determining whether the crack propagates. The problem is complicated by the fact that in many cases the mode mixity changes as the crack propagates.

LEFM can be used to characterise the crack growth not only in a homogeneous material, but also in the interface between dissimilar materials as shown in Fig. 2.

Suo [11, 12] expressed the stress field and the displacement field at the distance x behind the crack tip as a function of the stress intensity factor:

$$\sqrt{\frac{H_{11}}{H_{22}}}\delta_y + i\delta_x = \frac{2H_{11}K|x|^{\frac{1}{2}+i\varepsilon}}{\sqrt{2\pi}(1+2i\varepsilon)\cosh(\pi\varepsilon)} \tag{1}$$

$$\sqrt{\frac{H_{22}}{H_{11}}}\sigma_{yy} + i\sigma_{xy} = \frac{K|x|^{i\varepsilon}}{\sqrt{2\pi x}} \tag{2}$$
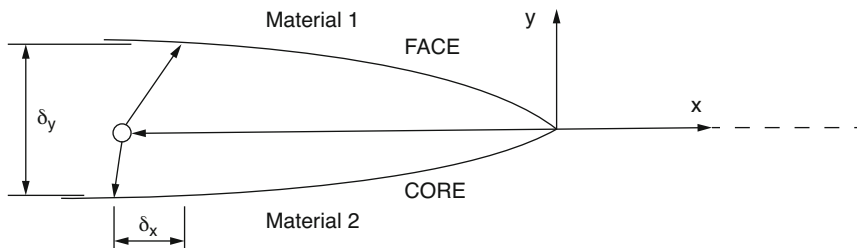
$$K = K_1 + iK_2 \; ; \; i = \sqrt{-1} \tag{3}$$

Fig. 2 Displacements at the interface of sandwich composites

Here the equations are complex, δ_y and δ_x are the relative opening and sliding displacements (see Fig. 2) of the crack flanks, σ_{yy} and σ_{xy} are the normal and shear stresses and H_{11}, H_{22} and ε are bimaterial constants given by:

$$H_{11} = \left[2n\lambda^{\frac{1}{4}}\sqrt{S_{11}S_{22}}\right]_1 + \left[2n\lambda^{\frac{1}{4}}\sqrt{S_{11}S_{22}}\right]_2 \tag{4}$$

$$H_{22} = \left[2n\lambda^{-\frac{1}{4}}\sqrt{S_{11}S_{22}}\right]_1 + \left[2n\lambda^{-\frac{1}{4}}\sqrt{S_{11}S_{22}}\right]_2 \tag{5}$$

$$\varepsilon = \frac{1}{2\pi}\ln\left(\frac{1-\beta}{1+\beta}\right) \tag{6}$$

$$\beta = \frac{\left[S_{12}+\sqrt{S_{11}S_{22}}\right]_2 - \left[S_{12}+\sqrt{S_{11}S_{22}}\right]_1}{\sqrt{H_{11}H_{22}}} \tag{7}$$

where n and λ are non-dimensional orthotropic constants, S_{ij} are components of the compliance matrix and β is Dundur's bi-material parameter [13]. The mode mixity phase angle and the strain energy release rate are described as [14, 15]:

$$\psi_K = \arctan\left[\frac{\mathrm{Im}\left(Kh^{i\varepsilon}\right)}{\mathrm{Re}\left(Kh^{i\varepsilon}\right)}\right] \tag{8}$$

$$G = \frac{H_{11}|K|^2}{4\cosh^2(\pi\varepsilon)} \tag{9}$$

Here $\mathrm{Im}(Kh^{i\varepsilon})$ and $\mathrm{Re}(Kh^{i\varepsilon})$ are the imaginary and real parts of the complex expression and h is an arbitrarily chosen characteristic length. In face/core interface crack problems, the characteristic length is often taken equal to the thickness of the debonded face sheets. The strain energy release rate and the mode mixity phase angle can also be expressed in terms of the relative opening and sliding displacements of the crack flanks:

$$G = \frac{\pi(1+4\varepsilon^2)}{8H_{11}|x|}\left(\frac{H_{11}}{H_{22}}\delta_y^2 + \delta_x^2\right) \tag{10}$$

$$\psi_F = \tan^{-1}\left(\sqrt{\frac{H_{22}}{H_{11}}}\frac{\delta_x}{\delta_y}\right) - \varepsilon\ln\left(\frac{|x|}{h}\right) + \tan^{-1}(2\varepsilon) \tag{11}$$

$$\psi = \psi_R = \tan^{-1}\left(\frac{\delta_x}{\delta_y}\right) \tag{12}$$

Here ψ_F and ψ_R are mode mixity phase angles respectively in the full and the reduced formulations. The reduced formulation of phase angle enables the correlation of phase angle values and the fracture modes; $\psi_R = 0°$ corresponds to the pure

mode I and $\psi_R = \pm 90°$ corresponds to pure mode II. The interface crack tends to propagate at the interface when $\psi_R \leq 0°$. In contrast, positive ψ_R promotes the deviation of the crack path, also known as kinking, into the core [16, 17].

2.2   Compliance and J-Integral Methods

For establishing the strain energy release rate from an interface material characterisation test with simple geometry it is often possible to use the compliance method. The compliance, C (the rate of increase of displacement with increase of applied load), is measured for a series of crack lengths, L, and the rate at which C increases with L, dC/dL, is estimated. The strain energy release rate is proportional to this, the relationship depending on the loading arrangement and the geometry of the specimen. For simple test arrangements the relationship is easily established analytically, but more complex geometries and arrangements require either a more complex analysis or a numerical model, such as a finite element model (FEM).

In the latter case, when FEM is used, it is often more convenient to use instead a method based on the path-independent J-integral, first defined by Rice [18]. An example of its application is described in Sect. 3.4.

For practical purposes, the compliance method is generally confined to problems where, except for a very local process zone at the crack tip, the specimen can be treated as linear-elastic. An advantage of the J-integral method is that, while it gives identical results to the compliance method for linear-elastic problems, it can also be used for non-linear and inelastic crack propagation problems, such as those involving fibre bridging.

2.3   Crack Surface Displacement Extrapolation (CSDE) Method

The Crack Surface Displacement Extrapolation (CSDE), introduced by Berggreen et al. [19, 20], is a relatively new finite element (FE) based mode mixity method to determine the energy release rate and mode mixity at a crack tip. In the analysis of cracked interfaces with large stiffness difference, the CSDE method has been shown by Berggreen [6], and also by the recent study by Barbieri et al. [55] described in Sect. 3.9, to be more robust and stable than other FE based mode mixity methods such as the Virtual Crack Closure Technique (VCCT) [21, 22]. The principle of the CSDE method is to calculate the energy release rate and mode mixity phase angle values based on the relative opening and sliding displacements of the crack flanks, Eqs. (10, 11 and 12), over a region behind the crack tip. The method subsequently finds a linear sub-region and extrapolates the values linearly over the numerical error
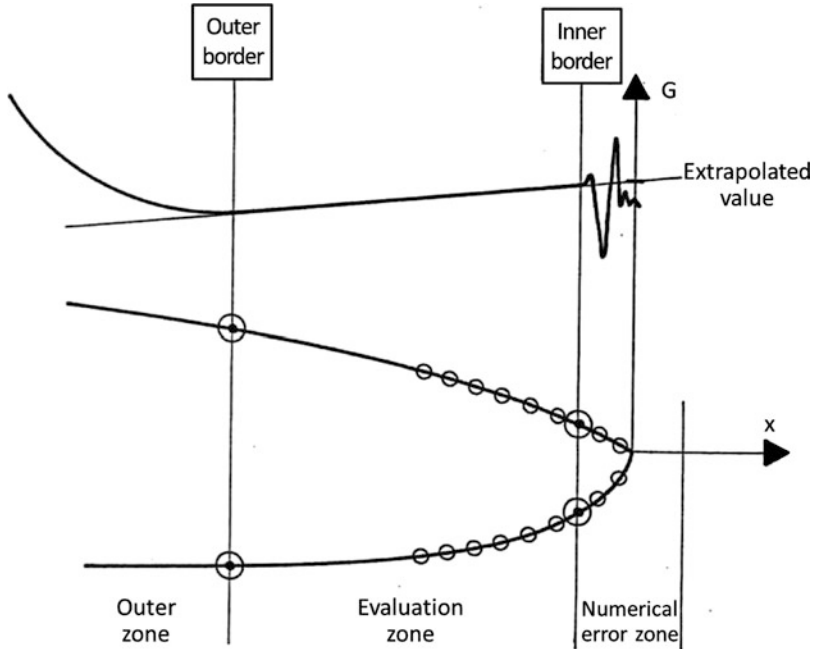
Fig. 3 The CSDE method presented schematically

zone to determine them at the crack tip, see Fig. 3. The energy release rate and mode mixity have been reported to express a physically impossible oscillatory behaviour close to the crack tip [23, 24]. The CSDE mode mixity method circumvents this behaviour, by extrapolating over the oscillatory region, which is often associated with large numerical errors in a finite element analysis.

2.4 Fatigue Crack Growth

The Paris law [25] can be expressed as a relationship between the rate of growth of a crack, da/dN, where a is the crack length and N the number of loading cycles, and the strain energy released per cycle, ΔG:

$$\frac{da}{dN} = C(\Delta G)^m \tag{13}$$

where C and m are constants that can be found from experiments.

2.5 The Cycle Jump Technique for Fatigue Crack Growth Calculation

In principle, once the fracture and crack growth properties have been obtained experimentally (Sect. 3) it is possible to model a real structure, with or without defects and damage, and estimate its fatigue life. However, in practice this can be extremely demanding and time-consuming. To overcome this problem, Moslemian et al. [26] modified the "cycle jump" technique for numerical analysis of fatigue crack propagation in a sandwich face-core interface that significantly reduces the computational effort. This is illustrated in Fig. 4, and consists essentially of the following steps:

1. Perform FE analyses of the damaged structure for a few cycles (using available mixed mode fracture data from fracture characterisation tests).
2. Fit spline curves to the development of deformations and key damage parameters with increasing number of cycles.
3. Extrapolate over a "jump" range of cycles to give a new, more advanced, assumed state of damage.
4. Repeat the process with this state as initial state.

The method was tested on 3D analysis of square sandwich panels with centrally located circular and elliptical debonds, and a concentrated normal force pulling the centre of the debonded face sheet away from the core [27], and validated against physical tests for a case with an initially circular debond [28]. It was also used by Martakos et al. [72, 74] in their studies of crack arresting devices reported in Sect. 4.6.
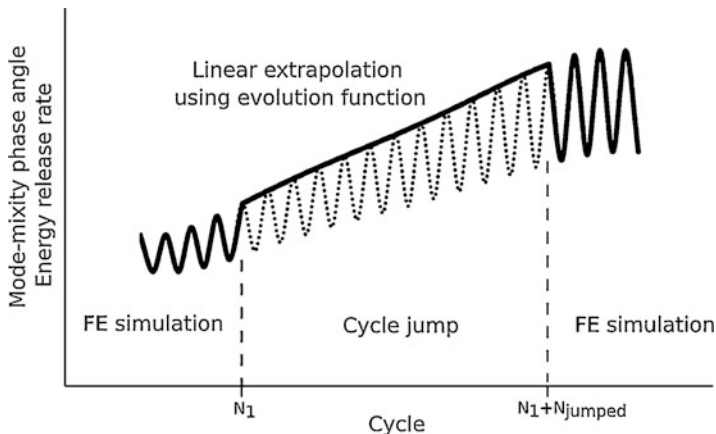

Fig. 4 Schematic of cycle jump technique

3 Experimental Fracture Characterisation Methods for Face/Core Sandwich Interfaces

3.1 Preliminary Remarks

Experimental methods for determining the fracture properties of face-core interfaces have been the subject of extensive research and development over the past 30 years; a significant part of this development has been supported by the ONR. The following subsections attempt to give an overview of the methods and the ways in which they have developed.

3.2 Cracked Sandwich Beam (CSB) Test

In sandwich panels under lateral pressure loading caused, for example, by slamming loads on the hulls of marine craft, the primary loading on the core is transverse shear. The ASTM C393 test [29] had long been used to determine the shear strength of sandwich core materials, but these tests do not consider the strength of the bond between the face sheet and core under the same loading. To address this, the cracked sandwich beam (CSB) specimen was developed and studied by Carlsson and co-workers [30, 31]. The test may be regarded as a development of the end-notch flexure (ENF) test used for determining the mode II interlaminar fracture properties of laminates. However, whereas the ENF specimen uses a crack at the mid-plane of a laminate, the CSB specimen requires the crack to be at the face-core interface and thus requires a different set of equations to extract the fracture properties.

Carlsson et al. [30] derived an expression for the compliance C of a sandwich beam under three-point bending with central load P, length $2L$ and width b having an end crack of length a. The mode II strain energy release rate G_{II} was then obtained using the relation

$$G_{II} = \frac{P^2}{2b} \frac{dC}{da} \tag{14}$$

3.3 Double Cantilever Beam (DCB) Test

Fracture at the face-core interface under peel loading (mode I) was addressed by Prasad and Carlsson [16, 17]. In [16], sandwich beam specimens were analysed using the finite element method. Peel fracture was studied using a modified double cantilever beam (DCB) sandwich specimen (Fig. 5) with a pre-crack between the face sheet and core, while shear fracture was studied with a modification of the
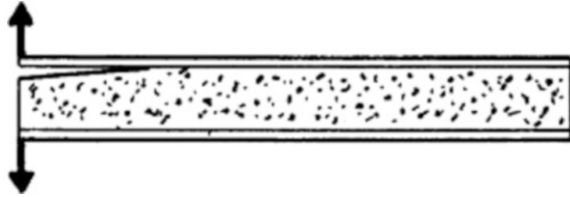
ASTM C273 block shear test [32] to include a face/core pre-crack. Complex and conventiona1 stress intensity factors were calculated for bimaterial cracks located between the face sheet and the bond layer and between the bond layer and the core over a large range of core moduli. Overall, much larger stress intensity factors were observed for an interfacial crack between the face sheet and bond layer than for a crack between the bond layer and core for both types of specimens. Crack kinking analysis of the DCB specimen revealed that the debond tends to remain interfacial for stiff core materials, but may deflect into the core for compliant core materials.

The same authors [17] experimentally examined bonding and crack kinking in sandwich beams, and also performed analysis using the finite element method. DCB and shear fracture specimens employing aluminium faces bonded to a wide range of PVC and PMI foam cores using two types of adhesives were considered. It was found that the Young's modulus of the core had a profound effect on the tendency of the face core interfacial crack to deflect (kink) into the core in DCB testing, while in shear testing crack kinking occurred for all core materials considered. Measured kink angles compared favourably with kink angles calculated based on the interfacial stress intensity factors prior to kinking.

Much later, Carlsson et al. [33] further investigated the crack path in foam cored DCB sandwich fracture specimens. A simple laminated beam analysis was presented for analysis of the propagation path of a core crack in both symmetric and unsymmetrical DCB sandwich fracture specimens with a polymer foam core. The analysis determined the sign of the shear stress ahead of the crack tip from the discontinuity of bending strain in the legs of the DCB specimen, and hence the kinking direction. The beam analysis, furthermore, assessed the stability of the crack path and provided the steady-state location of the crack after kinking (in the event of kinking). The analysis was in overall agreement with predictions of kink angle obtained from detailed finite element modelling and experimental crack paths in DCB specimens with an H100 foam core.

Aviles and Carlsson [34] presented an analysis of the compliance and energy release rate of the sandwich DCB specimen. They assumed that there was a starter crack at the upper face-core interface and that the crack remained at or near this interface during crack propagation. Beam, elastic foundation, and finite element analyses were presented and compared to experimentally measured compliance data, and compliance calibrated energy release rate (adjusted to eliminate the effect of the compliance of the test rig) over a range of crack lengths for foam cored specimens. It was found that the beam analysis provided a conservative estimate of the compliance and energy release rate. The elastic foundation model was in agreement with finite

element analysis and experimental compliance data. Recommendations for specimen design and an expression for an upper limiting crack length were provided.

3.4 Double Cantilever Beam Loaded with Uneven/Unequal Bending Moments (DCB-UBM)

3.4.1 Description

The double cantilever beam specimen with uneven, (or, unequal) applied bending moments (DCB-UBM) was first introduced by Sørensen et al. [35] for multilayer materials and later modified for sandwich composites by Lundsgaard-Larsen et al. [36], see Fig. 6. This specimen enables the investigation of fracture toughness at different mode mixity phase angles. Fracture analysis under linear elastic assumptions is carried out to calculate the energy release rate and mode mixity at the crack tip for isotropic and orthotropic materials. Pure moments are applied at the crack flanks while the other end of the specimen is held between the rollers. The design allows the application of loads with no transverse forces, so that the bending moment distribution is uniform throughout each of the three separate regions of the specimen: in the debonded part of the upper face sheet, in the combined core and lower face sheet over the same part of the length, and in the intact part of the sandwich beam. Thus stable crack growth is obtained. The DCB-UBM specimen is therefore G-controlled by nature, in the sense that the strain energy release rate is independent of the crack length.

Lundsgaard-Larsen et al. [36] applied the DCB-UBM test to the measurement of mixed mode cohesive laws for interfaces in sandwich structures. They increased the bending stiffness of the sandwich faces by bonding steel bars onto the sandwich faces. This stiffening reduces rotations and ensures that the method is applicable for thin face sandwich specimens. The J-integral was employed, and the opening of the pre-crack tip was measured using a commercial optical measurement system, from which mixed mode cohesive laws were extracted.

Closed-form expressions for the energy release rate, G, and mode mixity, ψ, for the DCB-UBM specimen have been derived by Kardomateas et al. [37] by means of a tri-material system similar to a sandwich construction. For the case of a

Fig. 6 Schematic illustration of DCB-UBM specimen
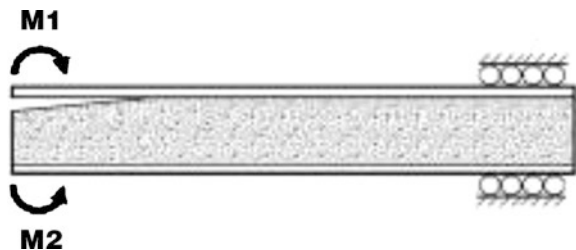
symmetrical layup, with identical, stiffened top and bottom face sheets, this was further developed more recently by Saseendran et al. [38], using the J-integral approach combined with laminate beam theory, to a five-layer model that includes the stiffener bars. The mode mixity, ψ, is derived in terms of a single scalar quantity ω which depends on the stiffnesses and thicknesses of the respective stiffener, face and core layers. The scalar parameter ω is obtained using, for example, finite element analysis (FEA). Therefore, for a specific face/core (or stiffener/face/core) interface system, FEA needs to be performed only once to map out ω for one loading configuration and the same ω can then be used for all other loadings as well. Effectively ω needs to be obtained for a range of typical component stiffness and thickness ratios and interpolation can then be used to obtain ω for a specific stiffness and thickness configuration.

The energy release rate and mode mixity for the DCB-UBM specimen can also be obtained using the CSDE method [20]. Geometrically linear analysis is performed on the specimen modelled with four-noded linear and eight-noded parabolic elements. The crack-tip mesh is highly densified and consists of numerically robust linear elements surrounded by a region of parabolic elements. Pure moments are applied at the ends of the crack flanks via master nodes in conjunction with multi-point constraint (MPC) elements, see Fig. 7.

The CSDE method calculates the strain energy release rate (ERR) and mode mixity phase angle ψ from the relative normal and shear crack flank displacements along the crack flanks within the parabolic elements close to the crack tip, and then extrapolates these values into the crack tip. The loading configuration for the experimental evaluation is selected according to the mode mixity at the crack tip obtained using the CSDE method.
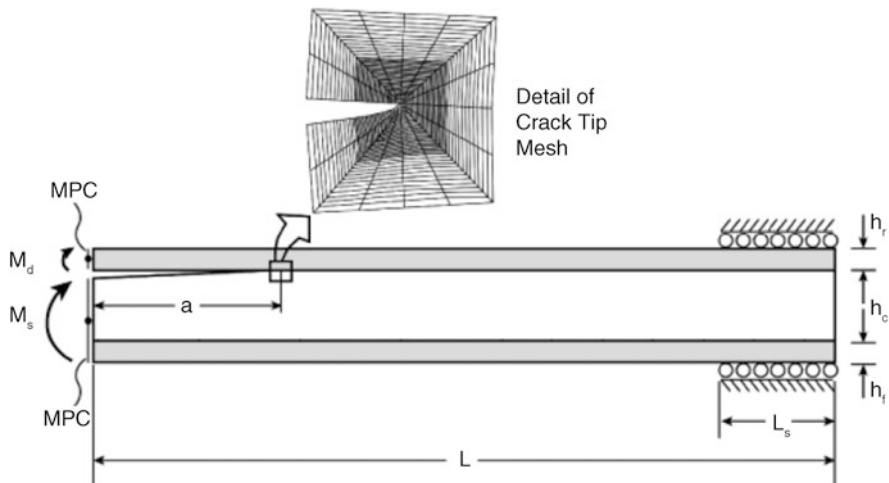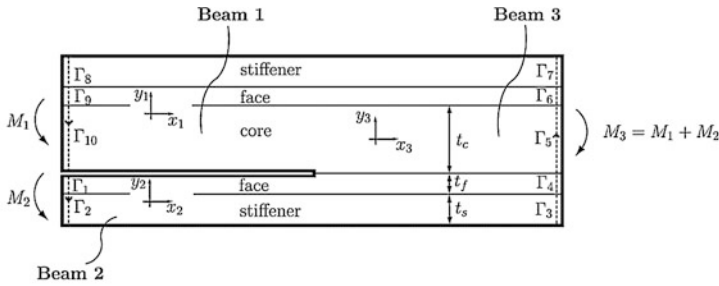

Fig. 7 FE model of DCB-UBM specimen

$$J = \sum_{p=1}^{10} \frac{\overline{E}_p M_b^2}{6(A_b D_b - B_b^2)^2} [A_b^2(y_{p-1}^3 - y_p^3) - 3A_b B_b(y_{p-1}^2 - y_p^2) + 3B_b^2(y_{p-1} - y_p)]$$

Fig. 8 Closed J-contour integral path for DCB-UBM multilayer specimen

3.4.2   DCB-UBM Specimen Design and Analysis

The thicknesses of the doubler layers are selected such that plastic deformation is prevented under the expected loads. In their study of cohesive laws (see Sect. 4.6) for interfaces with large-scale fibre bridging which violates the LEFM assumptions, Lundsgaard-Larsen et al. [36] selected the design based on the J-integral equation for the DCB-UBM specimen with doubler layers for a fixed moment ratio. However, in the LEFM regime the J-integral is equal to the strain energy release-rate, G. The J-integral was formulated as a function of extension, bending and coupling terms A, B and D, respectively, see Fig. 8 (which uses a slightly different configuration and notation from Saseendran et al. [38]).

  To measure a J-integral value, lower strength steel can be used with thick doubler layers. Using a thick doubler would, however, require the rig to apply high bending moments. Taking this into consideration, a trade-off is made between the strength and the thickness of the doubler layers. A thickness of 6 mm is chosen with a steel type with a yield strength of 750 MPa to characterise an interface with a fracture toughness of up to $J = 1500$ J/m^2.

3.4.3   Novel DCB-UBM Test Rig

The original DCB-UBM rig was loaded by wires and required a tall test frame. It was unable to perform fracture testing with cyclic loading conditions at a reasonable and practical frequency, and allowed only a limited range of phase angles. Berggreen et al. [39] presented a novel test set up that overcomes these shortcomings. A schematic of this test rig is shown in Fig. 9 and an assembly diagram in Fig. 10. The rig is capable of applying pure moments such that the asymptotic stress-field developed at the crack tip reflects the corresponding mode mixity. A conditional control system is implemented such that the ratio of the moments applied across the
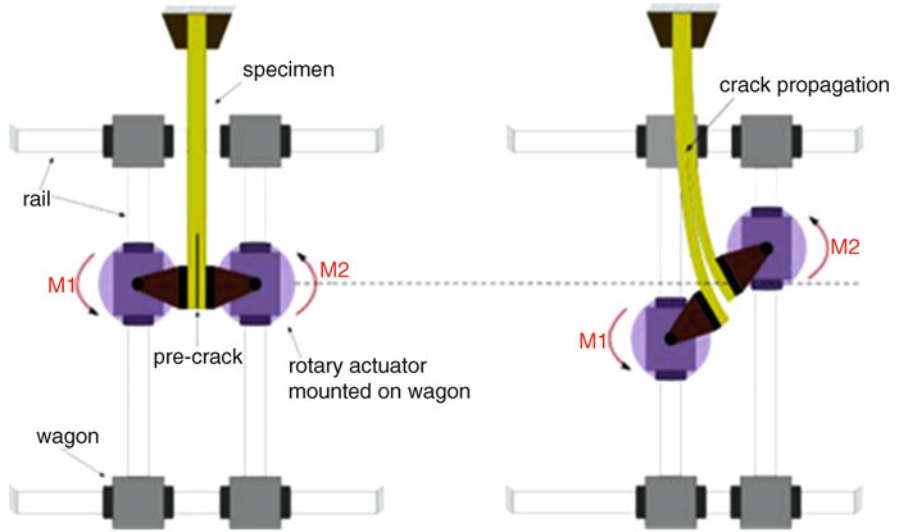
Fig. 9 Schematic illustration of DCB-UBM test rig
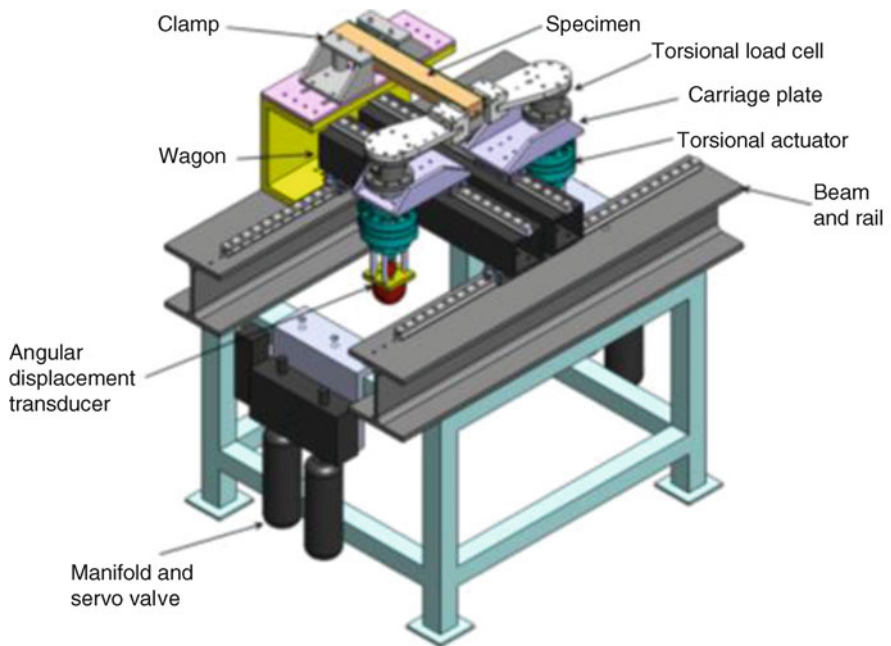

Fig. 10 Assembly drawing of the DCB-UBM test rig (isometric view)

arms remains constant, when controlling the test by increasing the angular rotations at the moment application points.

To apply the desired pure moments on each crack flank, two hydraulic rotational actuators are employed on either side of the specimen. These are equipped with torsional load cells and sensors to control the angular position of the actuators. A bi-axial servo-hydraulic controller is employed. To apply pure moments, the crack flanks must be able to deform without any constraints in the plane of deformation. This is achieved by mounting the actuators on pairs of rails which allow them to slide in the specimen plane (length-wise and width-wise). The specimen is held between roller supports, allowing it to slide in the length direction. This sliding ensures that there are no vertical forces on the specimen. The fixture does not have any restriction with regard to the type of specimens that can be tested. The steel doubler layers, however, require higher moments to bend the specimen to enable crack propagation for a particular moment ratio (MR). The extended steel arms engage in the fixture made on top of the torsional load cells (see Fig. 10). The moments are applied on each arm based on the defined moment ratios. The controller manipulates one rotational actuator such that the desired moment ratio is achieved. A conditional control ensures that, for a constant applied rotation rate in that actuator, the other actuator rotates keeping the moment ratio constant.

Note that, depending on the direction of opening of the arms, moment ratios can be positive or negative. A clear definition of the applied moment and sign convention is provided in Fig. 11, in which M_d is the moment applied on the debonded part and M_s is the moment applied at the substrate part. The FE model in Fig. 7 also shows the boundary condition due to the roller supports. The nomenclature for moments used here is the same as that used by Kardomateas et al. [37] in deriving the analytical expression for G for the DCB-UBM specimen. Thus, based on the direction of M_d and M_s, the sign of MR $= M_d/M_s$ changes. It should be noted that MR is positive if both M_d and M_s are clockwise or if they are both counter-clockwise, see Fig. 11.

Further details of the test rig are provided by Berggreen et al. [39]. They performed fracture testing on a typical marine grade sandwich configuration consisting of H45 PVC foam core and glass fibre face sheets to demonstrate the
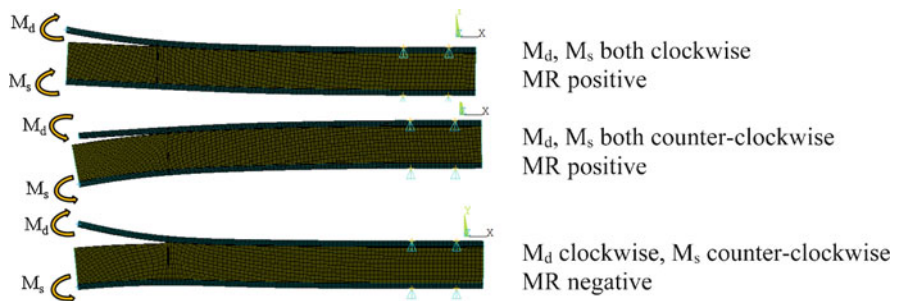

Fig. 11 Sign convention for moment ratio MR depending on applied moments M_d and M_s

applicability of the test method. The obtained fracture toughness agreed with interface toughness values in the literature measured using other test methods with the same material system. The effective kinematics of the test rig were measured using digital image correlation (DIC) by studying the rotations and moments of a specially designed calibration specimen and comparing the results against finite element results. The DCB-UBM specimen and test method were shown to be a promising candidate for obtaining face sheet/core interface fracture toughnesses in sandwich composites.

3.5   Tilted Sandwich Debond (TSD) and Modified TSD Specimens

For some face-core combinations and loading configurations a debond crack starting at the face-core interface deflects into the core, known as "kinking". To avoid this, a new test specimen for characterisation of debond failure of foam core sandwich structures, the tilted sandwich debond specimen (TSD), was proposed by Li and Carlsson [40–42] in a project carried out in collaboration between Florida Atlantic University (FAU) and KTH, and supported by the ONR Solid Mechanics Program. In the TSD test the bottom face of a sandwich is attached to an incline, and a vertical load is applied to the partially debonded top face (Fig. 12). In [40], Li and Carlsson examined the debond progression experimentally. For a sandwich consisting of glass/vinylester face sheets and PVC foam core, a critical angle of the incline, $\theta = \theta_c$, was identified. When $\theta < \theta_c$, it was found that an existing debond kinked into the core. The desired face/core debond failure occurred when $\theta \geq \theta_c$. It was observed that θ_c decreases with increasing crack length. The fracture toughness for debonding, expressed as the critical strain energy release rate, G_c, increased with increasing magnitude of the shear component.

In [41] the same authors analysed the TSD specimen using elastic foundation theory. The top face sheet was considered as a cantilever beam in the debonded region of the specimen and as a beam of finite length supported by an elastic foundation in the bonded region. An analytical model for the beam deflection was developed for design of the specimen, fracture analysis, and data reduction of face/

Fig. 12 The TSD specimen
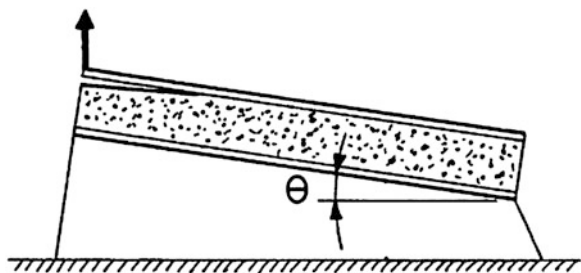
core debond toughness. A parametric investigation was conducted to examine how material and geometrical parameters of the constituents of the sandwich and test configuration influence the compliance of the TSD specimen. Testing was performed on a sandwich consisting of glass/vinylester face sheets over an H200 PVC foam core. The compliance predictions for this and a previously examined sandwich agreed favourably with experimental data over a large range of crack lengths and tilt angles. The debond toughnesses reduced from experimentally calibrated compliance and from the foundation model were consistent.

In [42] Li and Carlsson presented finite element analysis of several configurations of the TSD specimen, viz. a homogeneous and isotropic specimen, an interface crack specimen, and a sub-interface crack specimen. Stress intensity factors were determined using various mesh refinements over a range of tilt angles, and the mode mixity was related to the potential for kinking into the core. Irrespective of the tilt angle, it was found that cracks located at the face/core interface displayed a mode mixity favourable for kinking into the core. Experiments on a sandwich with an H100 PVC foam core revealed kinking at an angle in reasonable agreement with the prediction. After kinking, analysis of sub-interface crack configurations showed that the crack loading becomes highly mode I dominated, which indicates crack propagation parallel to the face/core interface, again in agreement with experimental observations. It was noted, however, that fracture mechanics analysis of foam materials, based on the assumption of a homogeneous material, becomes questionable when the singular domain becomes comparable to the cell size of the foam.

Viana and Carlsson [43], subsequently studied mode mixity and crack tip yield zones in TSD specimens with PVC foam core. Fracture mechanics analysis was conducted on core and debond fracture specimens. Five different PVC foam cores were examined. Stress intensity factors and the size of the plastic zone around the crack tip in foam core single-edge notch bend (SENB) and TSD specimens were estimated from the elastic displacements and stress fields near the crack tip. Analysis of the influence of core thickness and crack depth on the plastic zone size was performed on TSD specimens with H100 and R400 cores. It was found that the crack loading in the TSD specimen was essentially mode I, and that shear loading could not explain the higher toughness in the debond than the core. At the onset of fracture, the plastic zone height in the TSD specimen was much larger than that in a corresponding SENB specimen. It was believed that the plastic zone enlargement was a major factor explaining the elevation of debond toughness over the core toughness.

Viana and Carlsson [44] determined face/core debond toughness, expressed as the critical strain energy release rate (G_c), for sandwich specimens with composite and aluminium face sheets over various cross-linked PVC foam cores. Crack propagation occurred in the core, near the face/core interface for specimens with adequate face/core adhesion. Only for the highest density foam was it possible to propagate the crack in the immediate vicinity of the actual core/resin interface. The face/core debond toughness increased with increased foam density and reduced core thickness. For thick cores, the face/core toughness was independent of the core thickness.

A proposal for a modified TSD specimen was made several years later by Berggreen and Carlsson [45]. Analysis had shown that the range of phase angles that can be realised by altering the tilt angle and other parameters of the test is quite limited. To extend the range of mode mixities of the TSD specimen, a larger amount of transverse shear was introduced by reinforcing the loaded upper face with a stiff metal plate. Analysis showed that this method would extend the range of phase angles to a practically useful range. Guidelines on selection of thicknesses of the reinforcement, and design considerations for further modifications were provided.

Berggreen et al. [46] used the TSD test method, modified as above by reinforcing the loaded face sheet with a steel bar, to examine face/core debond fracture toughness of sandwich specimens with glass/polyester face sheets and H45 and H100 PVC foam cores over a large range of mode mixities. Fracture testing of the test specimens was conducted over a range of tilt angles. The fracture toughness exhibited mode mixity phase angle dependence, especially for mode II dominated loadings, while the fracture toughness remained quite constant for mode I dominated crack loadings. The fracture process was inspected visually during and after testing. For specimens with H45 cores the crack propagated in the core. For specimens with H100 cores, the crack propagated between the resin-rich layer and the face sheet.

3.6 Mixed Mode Bending (MMB) Specimen and Test

The mixed mode bending (MMB) specimen, originally developed and widely used for mixed mode delamination fracture characterisation of unidirectional monolithic composites, was extended by Quispitupa et al. [47] to the study of debond propagation in foam cored sandwich specimens (Fig. 13). The compliance and strain energy release rate expressions for the MMB sandwich specimen were derived based
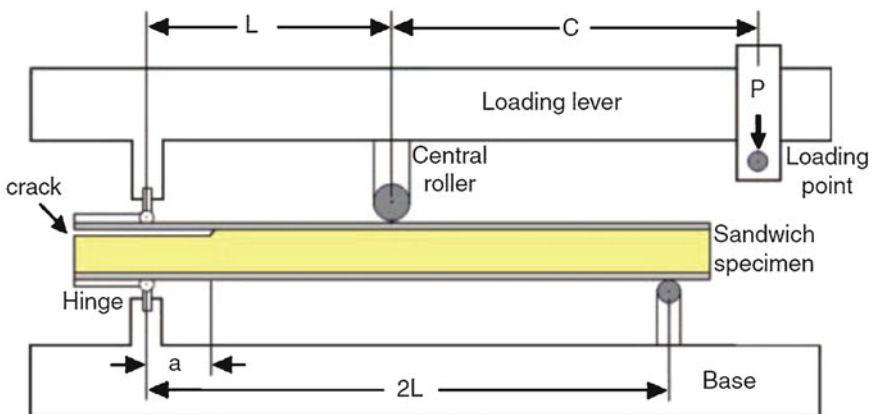

Fig. 13 MMB sandwich specimen and test arrangement

on a superposition analysis of solutions for the double cantilever beam (DCB) and cracked sandwich beam (CSB) specimens by combining a kinematic relationship for the specimen deformation with that of the loading provided by the test rig. This analysis provided also expressions for the global mode mixities.

The MMB compliance and energy release rate depend on the crack length, a, face and core thicknesses, h_f and h_c respectively, mechanical properties of the sandwich constituents (i.e. elastic modulus of the face sheet, E_f, and elastic modulus of the core, E_c), geometry of the specimen and loading conditions controlled by the lever arm distance, c. The analytical expressions for the MMB compliance C and energy release rate G can be written:

$$C = \left(\frac{c}{L} C_{DCB\_upper} + \frac{c-L}{2L} C_{DCB\_lower}\right)\left(\frac{c}{L} - \alpha\frac{c+L}{2L}\right) + \left(\frac{c+L}{L}\right)^2 C_{CSB} \quad (15)$$

$$G = \frac{P^2}{2b^2}\left(\begin{array}{l} \frac{c}{L}\left(\frac{c}{L} - \alpha\frac{c+L}{2L}\right)\frac{12}{E_f h_f^3}\left(a^2 + 2a\eta^{1/4} + \eta^{1/2}\right) + \\ \frac{c-L}{2L}\left(\frac{c}{L} - \alpha\frac{c+L}{2L}\right)\left[\frac{1}{h_c G_{xz}} + \frac{a^2}{(D-B^2/A)}\right] + \left(\frac{c+L}{L}\right)^2\frac{a^2}{8}\left(\frac{1}{D_{debonded}} - \frac{1}{D_{intact}}\right)\end{array}\right)$$

$$(16)$$

where b is the specimen width, L is the span between supports, and the decomposed compliance components are:

$$C_{DCB\_lower} = \frac{a}{b}\left[\frac{1}{h_c G_{xz}} + \frac{a^2}{3(D-B^2/A)}\right] \quad (17)$$

$$C_{DCB\_upper} = \frac{4}{E_f h_f^3 b}\left(a^3 + 3a^2\eta^{1/4} + 3a\eta^{1/2} + \frac{3}{2}\eta^{3/4}\right) \quad (18)$$

$$C_{CSB} = \frac{L^3}{6bD_{intact}} + \frac{L}{2h_c bG_{xz}} + \frac{a^3}{12b}\left(\frac{1}{D_{debonded}} - \frac{1}{D_{intact}}\right) \quad (19)$$

The load partitioning factor and elastic foundation modulus parameter can be expressed as:

$$\alpha = \left[\frac{\frac{a^3}{3}\frac{1}{(D-B^2/A)} + \frac{a}{k}\frac{1}{(G_f h_f + G_{xz} h_c)}}{\frac{a^3}{3}\frac{1}{(D-B^2/A)} + \frac{a}{k}\frac{1}{(G_f h_f + G_{xz} h_c)} + \frac{a^3}{3}\frac{1}{(E_f h_f^3/12)} + \frac{a}{k}\frac{1}{G_f h_f}}\right] \quad (20)$$

$$\eta = \frac{h_f^3 h_c E_f}{6E_c} \quad (21)$$

where k is the shear correction factor ($k = 1.2$). The stiffnesses A, B and D can be written as:

$$A = E_f h_f + E_c h_c \tag{22}$$

$$B = h_f h_c \left(\frac{E_c - E_f}{2} \right) \tag{23}$$

$$D = \frac{1}{12} \left[E_f \left(h_f^3 + 3 h_f h_c^2 \right) + E_c \left(h_c^3 + 3 h_c h_f^2 \right) \right] \tag{24}$$

$$D_{intact} = \frac{E_f h_f}{2} \left(h_c + h_f \right)^2 + \frac{E_f h_f^3}{6} + \frac{E_c h_c^3}{12} \tag{25}$$

$$D_{debonded} = (1 - \alpha) \left(D - B^2 / A \right) \tag{26}$$

A, B and D are the extensional, coupling and bending stiffnesses respectively, and $D_{debonded}$ and D_{intact} are the flexural stiffnesses of the debonded region and intact region of the cracked beam respectively. Further details are provided in [47].

An extensive parametric analysis to improve the understanding of the influence of loading conditions, specimen geometry and mechanical properties of the face and core materials was performed using the derived expressions and finite element analysis. The mixed mode bending compliance and energy release rate predictions were in good agreement with finite element results. The numerical crack surface displacement extrapolation (CSDE) method implemented in a finite element analysis was applied to determine the local mode mixity at the tip of the debond.

The same authors [48] presented a design analysis of the MMB sandwich specimen for face-core interface fracture characterisation. An analysis of the competing failure modes in the foam cored sandwich specimens was performed in order to ensure face-core debond fracture prior to other failure modes. This facilitates selection of the appropriate geometry for the MMB sandwich specimen to promote debond failure. An experimental study was performed using MMB sandwich specimens with an H100 PVC foam core and E-glass-polyester faces. Debond propagation was successfully achieved for the chosen geometries and mixed mode loading conditions.

In a third paper [49] the same authors presented an experimental study on face/core debond fracture of foam core sandwich specimens under a wide range of mixed mode loading conditions, using the MMB test arrangement. Sandwich beams with E-glass fibre-reinforced face sheets and PVC H45, H100 and H250 foam core materials were evaluated. A method was outlined to perform pre-cracking on fracture specimens in order to achieve a sharp and representative crack front. The mixed mode loading was controlled in the MMB test rig by changing the loading application point (and lever arm distance). Finite element analysis was performed to determine the mode mixity at the crack tip. The results showed that the face/core interface fracture toughness increased with increased mode II loading. Post-failure analysis of the fractured specimens revealed that the crack path depends on the mode mixity at the crack tip, the face sheet properties and the core density.

Manca et al. [50] examined face/core fatigue crack growth in foam-cored sandwich composites using the MMB test method. The mixed mode loading at the

debond crack tip was controlled by changing the load application point in the MMB test fixture. Sandwich specimens were manufactured using H45 and H100 PVC foam cores and E-glass/polyester face sheets. All specimens were pre-cracked in order to define a sharp crack front. The static debond fracture toughness for each material configuration was measured at different mode mixity phase angles. Fatigue tests were performed at 80% of the static critical load, at load ratios of $R = 0.1$ and 0.2. The crack length was determined during fatigue testing using the analytical compliance expression and verified by visual measurements. Fatigue crack growth results revealed higher crack growth rates for mode I dominated loading. For specimens with H45 core, the crack grew just below the face/core interface on the core side for all mode mixities, whereas for specimens with H100 core, the crack propagated in the core or in the face laminate depending on the mode mixity at the debond crack tip.

3.7   G-Control

A problem that arises with fatigue testing using the test methods described so far is that the cyclic energy release rate and crack propagation rate vary during the test. Manca et al. [51] presented a computer controlled testing methodology called "The G-control Method" which allows cyclic crack growth testing using real-time control of the cyclic energy release rate. The advantages of using this approach were described and compared with traditional fatigue testing methods (displacement or load control). The compliance based analytical formulation for G-control was explained for the DCB specimen and then applied to experimental testing of the sandwich MMB specimen. Experimental results were presented for sandwich MMB specimens with glass-epoxy face sheets and PVC foam core, showing that the G-control method allows fatigue testing at a constant range of energy release rates leading to a constant crack propagation rate.

Manca et al. [52] proceeded further to present experimental results from cyclic crack propagation tests performed on sandwich specimens with glass-epoxy face sheets and PVC foam cores using the G-controlled cyclic energy release rate (ΔG) test procedure. The face material was tested in tension, compression and shear to determine in-plane and out-of-plane mechanical properties, such as Young's modulus, Poisson's ratio and shear modulus. These properties were then used in an analytical model of the mixed mode bending sandwich specimen to calculate the compliance and energy release rate. Finite element analysis was used to determine the mode mixity of the crack loading. Experimental crack growth cyclic tests were carried out on pre-cracked MMB sandwich specimens with H45, H100 and H160 PVC foam cores under two mode mixities (mode I and mode II dominant). Postmortem analysis was performed on tested specimens, highlighting the influence of mode mixity and foam density on the crack path. Crack propagation diagrams showing da/dN versus ΔG curves were obtained to establish the Paris-Erdogan relation for each material combination tested at the two mode mixities (Fig. 14).
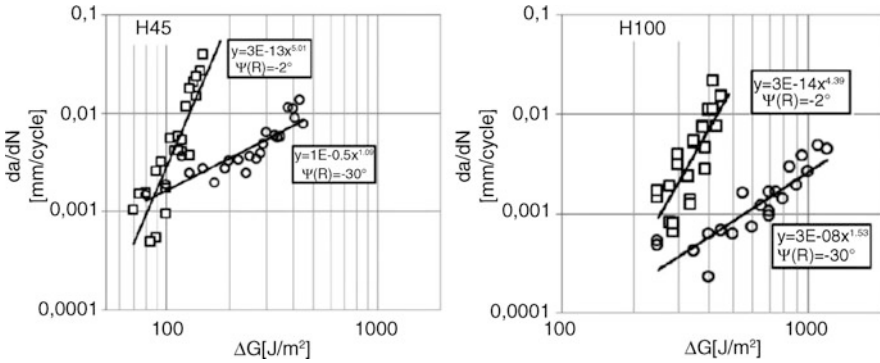
Fig. 14 *da/dN* versus ΔG for sandwich MMB specimens with GFRP faces and H45 and H100 cores tested at $\psi = 2°$ (mode I dominant) and $\psi = 30°$ (mode II dominant), from [52]
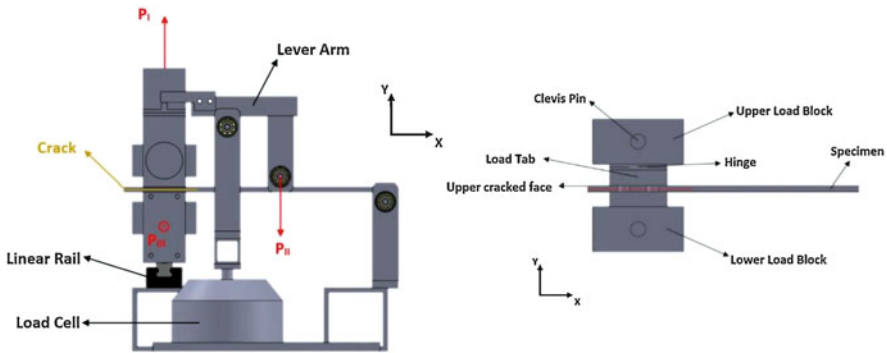

Fig. 15 Test rig for mode I-II-III testing of monolithic and sandwich specimens (schematic)

The results showed constant crack growth rates for all the materials tested and revealed the influence on mode mixity on crack propagation speed and foam density (higher foam density, slower crack propagation).

3.8 Shear-Torsion-Bending (STB) Test for Mixed Mode I-II-III Testing

Sabbadin et al. [53] report on a test machine, with associated test procedures, that has been under development to enable mixed mode I-II-III testing of cracked monolithic and sandwich specimens for fracture characterisation purposes. Thus it will cover the most general loading scenario where all three types of loadings at the crack tip are present. The test rig geometry (Fig. 15) is inspired by the STB test rig presented by Davidson and Sediles [54], whose experimental results agreed well with FEM

analyses regarding pure Mode III and multiaxial (Mode I + III, II and II + III) fracture characterisation of delaminated composite laminates.

3.9 Effects of Shear and Near Tip Deformations on Interface Fracture

In an ONR-supported collaboration between the University of Genoa, Italy, and DTU, Barbieri et al. [55] performed a theoretical study of the effects of shear and near tip deformations on the interface fracture properties of symmetric sandwich beams. The effects of shear on the energy release rate and mode mixity in a beam with isotropic layers and a debond crack at the face-sheet/core interface were investigated through a semi-analytical approach based on two-dimensional elasticity and LEFM. Expressions for the shear components of the energy release rate and mode mixity phase angle were obtained for sandwich beams with the necessary numerical coefficients derived through finite element analyses. The expressions were combined with earlier results for sandwich beams subjected to bending moments and axial forces to obtain solutions for general loading conditions and for an extensive range of geometrical and material properties tabulated in terms of non-dimensional, numerically obtained coefficients. The physical and mechanical significance of the terms of the energy release rate which depend on the shear forces were explained using structural mechanics concepts and introducing crack tip root rotations to account for the main effects of the near tip deformations. The results are applicable to laboratory specimens used for the characterisation of the fracture properties of sandwich composites, provided the lengths of the crack and the ligament ahead of the crack tip are above minimum lengths which are defined in the paper.

3.10 Low (Arctic) Temperatures

Farshidi [56] experimentally investigated the effects of low temperature on the face/core interface fracture toughness and the fatigue debond growth rate in foam core sandwich composites. Mixed mode bending (MMB) specimens were statically and cyclically tested using a compact testing fixture inside a climatic chamber at a low temperature ($-20\,^\circ$C) and at room temperature ($23\,^\circ$C). Testing was conducted at a mode mixity phase angle $\psi = 4.4^\circ$, very close to pure mode I (opening), and a mixed mode I/II (opening-sliding) mixed mode with $\psi = 23.9^\circ$. The fatigue test results were presented according to the modified Paris-Erdogan relation. The results showed substantial fracture toughness reduction at the low temperature (Fig. 16), on average 32% for the mode I case and 12% for the mixed mode case. The low temperature also increased the cyclic crack growth rate (Fig. 17) very significantly for the mixed mode case, but somewhat less for the mode I case.

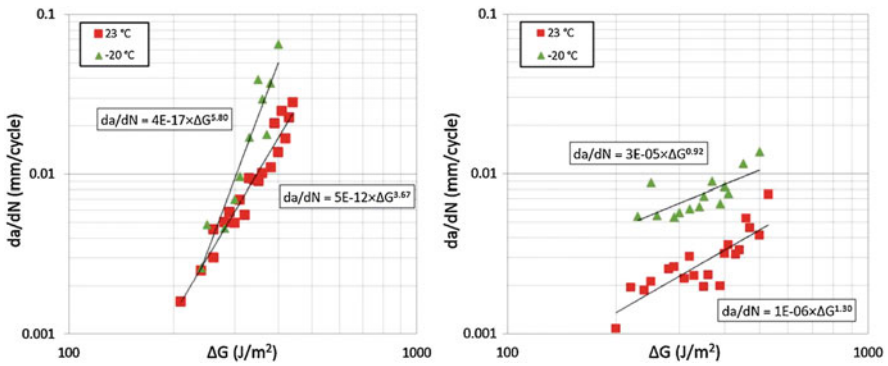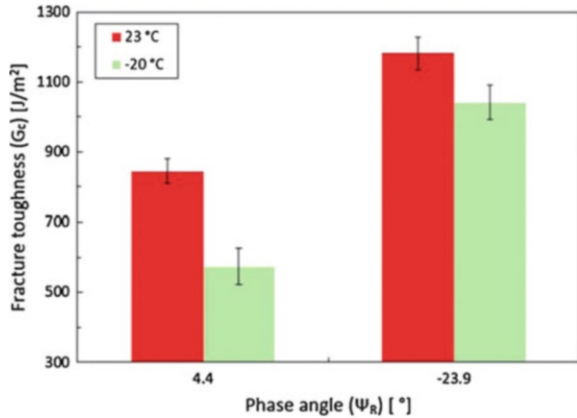**Fig. 16** Fracture toughness for two mode mixity phase angles and two temperatures

Fig. 17 da/dN versus ΔG results at $\psi_R = 4.4°$ (left) and $\psi_R = -23.9°$ (right)

4 Modelling and Testing of Sandwich Structural Components with Debonds

4.1 Curved Beams with Debonds

Layne and Carlsson [57] considered the problem of a curved sandwich beam under loading that tends to straighten the beam. Each beam was made with glass-polyester faces and a PVC foam core, and consisted of a 90° circular arc with straight legs to either side. The beams were tested in four-point bending in the direction tending to straighten the beam. The mode of failure was debonding of the face sheet on the convex (outer) side, suggesting that weaknesses in the bond were critical. The same authors [58] then tested similar curved beams with artificial debonds under similar loading. These beams suffered marginal reductions in stiffness, but substantial reductions in strength due to the presence of a debond.

4.2   Debonded Sandwich Columns in Axial Compression

In an early ONR-supported study, Aviles and Carlsson [59] developed an elastic foundation model for analysis of the local buckling behaviour of foam core sandwich columns containing a full-width face/core debond. They performed parametric studies to evaluate the effect of debond length, core thickness, core density, face sheet thickness, face sheet modulus and boundary conditions, on the local buckling load. They compared model predictions with experimental results obtained for sandwich specimens made from glass/vinylester face sheets and various PVC foam cores containing face/core debonds. The predictions were in reasonable agreement with measured buckling loads. Note that this study was confined to buckling of the face sheet, and did not consider crack propagation.

As part of the work performed under the Network of Excellence on Marine Structures (MARSTRUCT), partially funded by the European Union, Moslemian et al. [60] examined the failure of compression loaded sandwich columns with a full-width face/core debond. Tests were conducted on sandwich columns with glass/epoxy face sheets and H45, H100, and H200 PVC foam cores in a specially designed test rig. The strains and out-of-plane displacements of the debonded region were monitored using the digital image correlation technique. Finite element analysis and LEFM were employed to predict the critical instability load and compression strength of the columns. The energy release rate and mode mixity were determined and compared to fracture toughness data obtained from TSD tests, predicting propagation loads. Instability loads of the columns were determined from the out-of-plane displacements using the Southwell method. The finite element estimates of debond propagation and instability loads were in overall agreement with experimental results. The proximity of the debond propagation loads and the instability loads showed the importance of instability in connection with the debond propagation of sandwich columns.

Most of the columns with H200 core and some columns with H100 failed by debond propagation at the face/core interface towards the column ends. Bifurcation buckling instability of the debonded face sheet was not observed before the debond propagation initiated. It is believed that the initial imperfections are mostly responsible for this behaviour, which is similar to compression loading of a curved beam. Slight kinking of the debond into the core was another failure mechanism which occurred in columns with a low density H45 core. Compression failure of the face sheet occurred in all specimens with H200 cores and a 25.4 mm debond, which can be explained by the proximity between the debond propagation and the compression failure load of the face sheet. Instability and crack propagation loads of the columns were predicted based on geometrically nonlinear finite element analysis and linear elastic fracture mechanics. Testing of modified TSD specimens was conducted to measure the fracture toughness of the interface at the calculated phase angles for the column specimens associated with the debond propagation. Comparison of the measured out-of-plane deflection, instability, and debond propagation loads from experiments and finite element analyses showed fair agreement. For most of the

investigated column specimens, it was shown that the instability and debond propagation loads are very reasonable estimates of the ultimate failure load, unless other failure mechanisms occur prior to buckling instability.

4.3 Debonded Sandwich Panels in Axial Compression

As part of the SaNDI Project referred to elsewhere in this chapter, Nøkkentved et al. [61] studied face/core debond-damaged sandwich panels exposed to non-uniform, in-plane compression loads. The study primarily concerned experimental methods, but simple finite element calculations were also applied. The specimens were rectangular, 580 mm × 800 mm, with 3.2 mm thick faces and 45 mm thick cores. Eight specimens had Divinycell H80 (80 kg/m^3) structural cross-linked PVC foam cores and two had H200 (200 kg/m^3) cores. The faces each had two 300 g/m^2 layers of chopped strand mat and two of 850 g/m^2 non-crimp quadri-axial fabrics, placed symmetrically about the midplane of each face. Seven of the specimens were fabricated with circular debonds between the core and one face sheet with diameters 100, 200 and 300 mm. Three additional specimens were intact prior to testing. The debonded panel area was manufactured by substituting the adhesive polyester with uncured polyester, covered by a thin paper sheet before applying the face layer. All the panels were reinforced at the edges. The complexity of applying a controlled non-uniform compressive load to the test panels required a strong focus on the development of a suitable test rig. The experimental results showed a considerable strength reduction with increasing debond diameter, with failure mechanisms varying between fast debond propagation and wrinkling-induced face compression failure for large and small debonds, respectively. A comparison between a simple numerical model and the experimental results showed fair agreement.

Berggreen and Simonsen [19] described the development, validation and application of a FEM based numerical model for prediction of residual strength of damaged sandwich panels. At the heart of the theoretical approach was the CSDE method (Sect. 2.3). The method was able to predict the maximum load carrying capacity of real-life panels with debond damage, where the failure is governed by face-sheet buckling followed by debond growth. The method was first developed in 2D and then extended to 3D by use of a number of realistic assumptions for the considered configurations. Comparison of the theoretical predictions with the series of panel experiments described in [61] showed that the model was able to predict the failure modes and the residual strength of damaged panels with accuracy sufficient for practical applications.

In an extension of the SaNDI Project aimed at generating strength reduction data for a specific series of naval vessels, with support of the Royal Norwegian Navy, Moslemian et al. [62] studied the failure of compression-loaded sandwich panels with implanted, circular face/core debonds. Uniform compression tests were conducted on intact sandwich panels with three different core materials (H130, H250 and PMI) and on similar panels with circular face/core debonds having three different diameters.
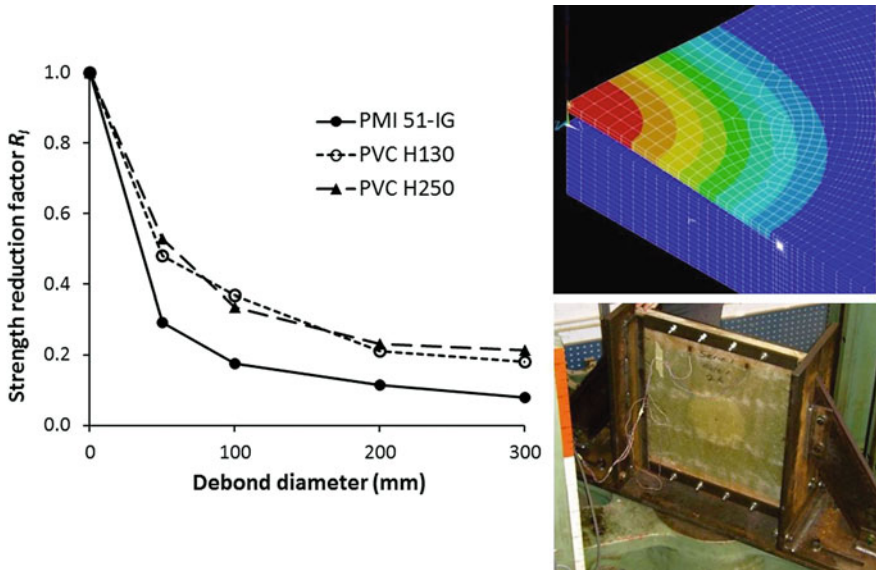
Fig. 18 Local strength reduction factors for face-core debond damage on sandwich layups with GFRP face sheets and three different foam core materials, with in-plane compressive loading [62]

The strains and out-of-plane displacements of the panel surface were monitored using the DIC technique. Mixed mode bending (MMB) tests were conducted to determine the fracture toughness of the face/core interface of the panels. Finite element analysis and LEFM were employed to determine the critical buckling load and compression strength of the panels. Numerically determined crack propagation loads in most of the cases showed a fair agreement with experimental results, but in a few cases up to 45% deviation was seen between numerical and experimental results. This can be ascribed to several factors such as the large scatter in the measured interface fracture toughness, and differing crack tip details and crack growth mechanisms between the panels and the MMB specimens. Tentative strength reduction curves were presented (Fig. 18), but uncertainty concerning the intact strengths of the materials used needs to be removed before these can be utilised with confidence.

At approximately the same time as the above studies, Aviles and Carlsson [63–66], with ONR support, also conducted studies of the compression strength of sandwich panels containing debonds. In [63] they conducted an experimental study of local buckling and failure behaviour of compression-loaded sandwich panels containing one-sided, centrally located circular and square face/core debonds. Sandwich panels with 2 mm thick glass/epoxy face sheets and a range of PVC foam cores were prepared (and also some with balsa cores). The core thickness was 25 mm in most cases, but some had 12.5 mm and 50 mm thick cores. The panels were 150 mm wide and 200 mm long. Note that these panels were appreciably smaller in scale than those considered by Moslemian et al. [62]. The face modulus and Poisson's ratio were: $E_f = 20.6$ GPa and $\nu_f = 0.42$. The foams were assumed to be

isotropic with a Poisson's ratio $\nu_c = 0.32$, and Young's moduli of 40, 100 and 200 MPa for the H45, H100 and H200 foams, respectively. A face/core debond was introduced in each panel by implanting a thin (30 μm thick) Teflon film between one face sheet and the core, at the centre of the panel. The circular debonds were 50, 63, 75, and 100 mm in diameter.

A test fixture similar to that used by Moslemian et al. [62] (see Fig. 18) was developed for uniaxial compression loading of the test panels, of nominal size 200 × 150 × 30 mm (length × width × thickness) with some flexibility to accommodate other dimensions. Strain gauges were bonded on both face sheets at the panel centre to enable monitoring of the strains during loading. Three replicate panel specimens were tested.

The local buckling load was determined from the bifurcation point in the load-strain response. At the point of local (face) instability, a strain reversal was observed for the debonded face sheets. A rapid decrease in load after face buckling was indicative of a lack of post-buckling strength. Hence, this type of damage can be very serious in compression-loaded panels in a sandwich structure.

The same authors presented first a 2D elastic foundation [64] and then a 3D finite element [65] analysis of the buckling behaviour. In the latter, experimentally measured local buckling loads for the panels with H45, H100, and H200 cores and a range of debond sizes from [63] were compared to predictions from the 3D finite element analysis. For the panels with H45 core, the agreement between FEA and experiments was quite favourable. For higher density cores there was agreement for smaller debonds, but for larger debonds the FEA was conservative. The under-prediction of the critical load for large debonds was believed to be due to the way the debonds were artificially generated in the experimental study by insertion of a Teflon film. Such films may adhere to the resin and core after resin infusion resulting in tractions preventing the opening of the debond. The tendency for such problems was more pronounced for large debonds.

The experimental observations revealed that failure was initiated by local buckling of the debonded face sheet. After buckling, the debond rapidly propagated transversely to the loading direction followed by the collapse of the panel.

Aviles and Carlsson [66] also analysed the face/core debond propagation using a fracture mechanics approach. A three-dimensional, geometrically nonlinear finite element model of the debonded panel was combined with LEFM to determine the stress intensity factors and energy release rate at the debond (crack) front parallel and perpendicular to the applied load to predict initiation of debond propagation. The solution for the near tip crack flank displacements derived by Suo [11] was utilised to extract the stress intensity factors K_I and K_{II} from the relative opening and sliding displacements of the crack flanks. A range of core densities and debond sizes were analysed. Mode I was found to dominate the fracture process. The critical load for crack propagation predicted using fracture mechanics concepts was found to agree with measured collapse loads for smaller debonds, but fell below measured debond propagation loads for larger debonds. In all cases the predicted direction of crack propagation was perpendicular to the loading direction, in agreement with the experimental observations.

4.4 Debonded Sandwich Panels under Lateral Pressure Loading

As part of the SaNDI Project, Jolma et al. [67] developed and applied a tool for assessing residual strength of debond damaged laterally loaded sandwich panels. The analysis tool consisted of a parametric finite element model and a fracture mechanics calculation procedure to determine the residual strength. The parametric approach allowed variation of all geometric and material entities. The fracture mechanics calculation used crack flank displacements obtained from the finite element analysis solution and experimentally measured mixed mode fracture toughness values to determine the ultimate failure load. The analysis tool was validated with a number of different ship type panels by comparing the results from the tool with those from panel experiments. The analysis tool predicted both failure load and failure mode well. It was noted that the tool could be used to determine the residual strength of different damage cases and had a considerable potential for further development.

4.5 X-Joints under Fatigue Loading: STT Test Feature

In a Danish project concerned with improving damage tolerance of sandwich structures, Moslemian and Berggreen [68, 69] investigated face/core fatigue crack growth in sandwich X-joints numerically and experimentally. In the first part of the study [68] they presented an experimental investigation of fatigue crack growth and characterisation of the face/core interface of the joints. Sandwich tear test (STT) specimens with a face/core debond representing a debonded sandwich X-joint were tested under cyclic loading. Fatigue tests were conducted on the sandwich tear test specimens with H45, H100 and H250 PVC cores and glass/polyester face sheets. The digital image correlation (DIC) technique was used to locate the crack tip and monitor the crack growth. For the specimens with H45 core, unstable crack growth took place initially. Following the unstable propagation, the crack propagated in the core underneath the resin-rich cell layer approaching the interface. However, the crack did not kink into the interface. For the specimens with H100 core, the crack propagated initially in the core and then returned into the interface and continued to propagate in the interface. For the specimens with H250 core, the crack initially propagated in the core and then kinked into the interface. The interface crack eventually kinked into the face sheet, resulting in large-scale fibre bridging. Finally, mixed mode bending (MMB) tests were conducted to measure crack growth rates of the face/core interface at mode mixity phase angles similar to those calculated for the STT specimens.

In the second part of the study [69] the same authors attempted to simulate the fatigue crack growth in the same tested STT specimens using the finite element method. To accelerate the simulation, the cycle jump method (Moslemian et al. [26])

described in Sect. 2.5 was utilised and implemented in the finite element routine. This method is based on conducting finite element analysis for a set of cycles to establish a trend line, extrapolating the trend line spanning many cycles, and using the extrapolated state as initial state for additional finite element simulations. The measured *da/dN* relations of the face/core interface in Part I [68] were used as input to the fatigue crack growth simulation routine. A fair accuracy with 99% saving in computation time was achieved in the simulation of the STT specimens with H100 core. However, for the specimens with H45 core a large deviation between the numerical and experimental results was seen due to a partially unstable fatigue crack growth which was not taken into account in the simulations.

4.6 Improving Damage Tolerance

As noted in earlier sections, a face/core debond in a sandwich structure may propagate in the interface or kink into either the face or core. In a Danish project, partly funded by the European MARSTRUCT Network of Excellence, Lundsgaard-Larsen et al. [70, 71] examined various modifications of the face/core interface in foam core sandwich specimens and found that certain modifications of the face/core interface region influenced the kinking behaviour. They used finite element analysis and testing of sandwich DCB-UBM specimens with a range of mode mixities (between modes I and II) to develop a cohesive zone model of the fracture process including large-scale fibre bridging. Use of the DCB-UBM specimen enabled accurate measurement of the J-integral as the crack propagated. By altering the mode mixity of the loading, the crack path could be changed so that it deflected from the interface into the adjacent face or core. The transition points for crack kinking were identified and the influence of four interface design modifications on the propagation path and fracture resistance were investigated.

The authors investigated the use of a chopped strand mat (CSM) and of a continuous filament mat (CFM) placed between face and core, a layer of woven fabric between the face and CSM, and stitching of the layers of the face laminate. In addition, the effects of core material (comparing H200 with H130 density PVC foam) and specimen width were examined. The highest overall toughness was achieved with the CFM layer, although kinking into the face occurred at relatively low mode mixity. The mode mixity range where the crack propagated in the face/ core interface region could be extended by the woven fabric layer placed adjacent to the face. Stitching prevented kinking of the crack into the face layers and provided overall high toughness. The specimens with a lower density core (H130) failed by crack kinking into the core at low mode mixities, and overall the debond toughness was much less than for the H200 core. The fracture toughness increased with specimen width as a result of more bridging fibres participating in the fracture process.

In a collaboration between DTU, Aalborg University, the University of South-ampton, Siemens Wind Power A/S, and LM Wind Power Blades A/S, Martakos

et al. [72] embedded a novel, pre-moulded polyurethane resin crack arresting (peel stopping) device in sandwich panels. They tested the panels under out-of-plane loading applied to the sandwich panel face-sheets. Fatigue crack propagation was induced in the face-core interface of the sandwich panels which met the crack arrester. The effect of the embedded crack arresters was evaluated in terms of the achieved enhancement of the damage tolerance of the tested sandwich panels. A finite element model of the experimental setup was used for predicting propagation rates and direction of the crack growth. The FE simulation was based on LEFM and a Paris law for crack propagation to predict the residual fatigue life-time and behaviour of the test specimens. Finally, a comparison between the experimental results and the numerical simulations was made to validate the numerical predictions as well as the overall performance of the crack arresters. In [73, 74] they investigated and optimised, using both numerical modelling and experiments, an alternative, simpler device using the STT tearing specimen.

5 Damage Tolerance and Assessment Procedures for Naval Sandwich Vessels

5.1 Introduction

Fundamental research concerning face-core debonds in sandwich structures mainly considers the development of damage in simple beam specimens of various types, and derivation of material and interface fracture properties from these tests, as described in Sect. 3. These simple beams only partially resemble real sandwich structures in ships, which generally consist of an assembly of sandwich panels (flat and/or curved), in some cases stiffened by beam-like structural components. For static loading, and to some extent impact and shock loads, fairly extensive physical testing and numerical modelling have been performed on sandwich panels under appropriate in-plane and out-of-plane loading, some of which has been described in Sect. 4. However, under cyclic fatigue loading, only very limited testing and modelling have so far been performed on real, three-dimensional structures such as panels or more complex configurations.

In principle, once the fracture properties have been obtained it is possible (e.g. for the vessel owner or operator) to model a real structure, with or without defects and damage, and estimate its residual strength and/or fatigue life. However, in practice this can be an extremely demanding and time-consuming task, especially with regard to fatigue life. Furthermore, the owner/operator needs to be able to assess the consequences for the operation of the ship when subjected to both local and global loads. Thus there is a need for an integrated defect/damage assessment system that can be used by others than research specialists.

Based on consideration of residual static strength immediately following damage, procedures for evaluating damage tolerance of sandwich hull structures have been

established previously in the SaNDI Project referred to in Sect. 1 and subsequent extensions of that work. These procedures have varying degrees of simplification, and some can be readily used by the crew on board a ship for decision-making.

In Sects. 5.2, 5.3 and 5.4 an overview is provided of the damage assessment scheme developed in the SaNDI Project (2001–4) for static strength, and of simplifications and formulations made subsequently for on-board use in a specific naval application. Then, in Sects. 5.5 and 5.6, possible procedures to evaluate damage growth under cyclic loading following accidental damage are discussed.

5.2   The SaNDI Project: Background and Aims

The SaNDI Project, JP3.23 Inspection and Repair of Sandwich Structures in Naval Ships, has been briefly described in Sect. 1. The objectives were to develop methodologies for both production control and damage inspection for naval sandwich structures, and in particular to give improved knowledge of how defects and damage affect structural performance and to establish acceptance criteria for defects and damage. In addition, detailed studies were made of relevant NDI (non-destructive inspection) and monitoring techniques as well as repair methods. The main deliverables were two manuals that could be used as a basis for developing inspection and repair handbooks for specific vessels, focusing respectively on production defects and in-service damage [2–5].

Production defects and in-service damage types that are relevant for naval sandwich structures were listed in Sect. 1; most of these were addressed in the SaNDI project. Face-core debonds may occur during production as a result of contamination of the face and core surfaces or poor control of ambient conditions. They may also occur (or become evident) during service as a result of unfavourable events or environmental conditions. In particular, debonds may result from impact damage (if the core is damaged), from core shear cracking or from pull-off effects at out-of-plane joints between panels (such as sometimes occur where a deckhouse is attached to a deck). This last case is essentially the same as the situation represented by the STT specimen in the study of X-joints in Sect. 4.5.

If a naval vessel experiences damage while in operation, it may be necessary to make urgent decisions regarding corrective actions. Analysis of damage and its structural consequences can be a time-consuming and demanding task that takes many hours or days to perform. Thus it is desirable to have as much data already available that can be quickly accessed and processed. With this in mind, the participants in the SaNDI Project developed procedures that could use almost exclusively pre-calculated information, stored in a systematic format and readily available in decision support tools and/or manuals on board a ship and at its onshore support facilities. The data and procedures have since been further refined and developed in the context of a specific series of all-sandwich composite vessels. Similar data and procedures can also be applied to defects arising during production.

5.3 Details of the SaNDI Approach to Damage Assessment Based on Residual Strength

In proposing ways of assessing the consequences of damage it was found convenient to define four levels of damage in a structure made up principally of sandwich panels connected at their edges:

- *Level 1 damage*: Small local damage. Covers a small part of an individual panel. The influence of the damage on the panel stiffness and the stresses at remote points on the panel can be neglected.
- *Level 2 damage:* Medium local damage. Confined to one panel but does not meet the requirements for level 1 damage. The stiffness of the panel is not significantly influenced by damage. Redistribution of stresses in the global structure can be neglected in assessing the reduction of global ship strength.
- *Level 3 damage*: Large local damage. Confined to one panel but does not meet requirements for level 1 or level 2 damage. The stiffness of the panel is significantly influenced by the damage. Redistribution of stresses in the global structure cannot be neglected.
- *Level 4 damage*: Extensive damage. Affects two or more panels and/or supporting structure. Generally leads to extensive redistribution of stresses in the remaining structure and possibly severe overloading of adjacent parts. Must be analysed at the global ship level.

When considering the consequences of damage it is relevant to consider three different scales in the structure: the local scale (only relevant for level 1 damage), the panel scale and the global ship scale. At each of these scales it is possible to define a strength reduction factor defined as in Table 1.

For several level 1 and some level 2 damage cases, plots were developed showing the way the residual strength decreases with the size of the damage. These plots were derived for specific sandwich layups using analytical/numerical modelling and supported by laboratory tests. Such plots are conveniently constructed with the dimensionless local strength reduction factor R_l or panel strength reduction factor R_p plotted against damage size, though in some cases it can be difficult to decide on

Table 1 Three scales to be considered when assessing damage in a naval sandwich structure

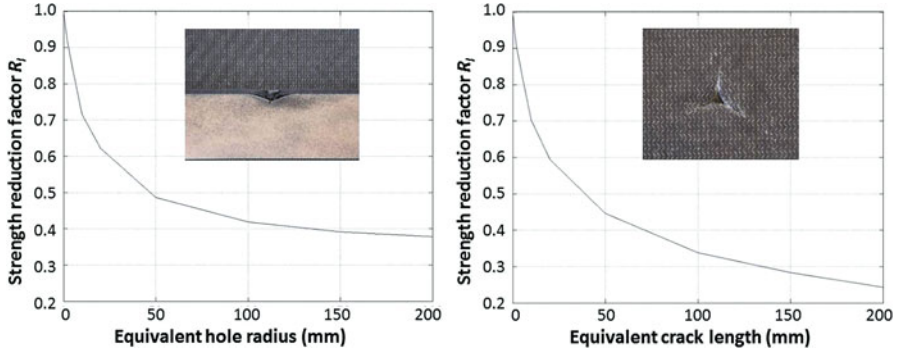| Schematic	Scale	Strength reduction factor
	Local	$R_l = \dfrac{\text{Nominal (far field) stress or strain to cause failure with damage}}{\text{Nominal (far field) stress or strain to cause failure without damage}}$
	Panel	$R_p = \dfrac{\text{Maximum allowable load on damaged panel}}{\text{Maximum allowable load on intact panel}}$
	Ship	$R_s = \dfrac{\text{Maximum allowable load on damaged ship}}{\text{Maximum allowable load on intact ship}}$

Fig. 19 Local strength reduction factors for face sheet impact damage on a sandwich layup with CFRP face sheet and PVC foam core, with in-plane compressive loading. Blunt impact (left) and sharp impact (right). The curves were obtained with the aid of equivalent hole and crack models

an intact strength value to use in the denominator. Figure 19 shows such curves plotted for two cases with local CFRP face sheet impact damage [5], while Fig. 18 in Sect. 4.3 shows corresponding curves for debond damage on sandwich layups with GFRP faces and three types of foam core, from a later, more comprehensive study [62]. Both figures, and a study at DTU of the effects of face sheet wrinkle defects [75] relate to in-plane compressive loading, which was the main focus in the SaNDI Project. However, some studies on tensile loading have been investigated more recently and the results for face sheet impact damage extended to GFRP face sheets [76]. In the studies of face sheet impact damage, blunt and sharp impacts were studied with the aid of equivalent hole and crack models, respectively, combined with laboratory testing.

Note that use of the local strength reduction factor R_l assumes that the damage size is much smaller than the in-plane panel dimensions. When the local factor R_l is used, it can be combined with a local location and load type sensitivity factor S_p, to give the panel strength reduction factor R_p:

$$R_p = R_l S_p \text{ with a maximum value of } 1.0. \tag{27}$$

The factor S_p is defined as the ratio of the value of the load on the panel that would cause the critical stress or strain component at the damage location to reach its maximum allowable value, *ignoring the damage*, to the maximum allowable value of load on the intact panel (i.e. the load that causes the critical stress or strain component to reach its maximum allowable value at the most highly stressed or strained location). This reflects the fact that, even if parts of the panel are at their design strength limit under the maximum design loading, some other parts may be less severely stressed and thus able to sustain damage without consequences for the panel as a whole. Note that the variation of S_p over the panel depends on the type of loading to which the panel is subjected and also the panel boundary conditions. By definition,

$$S_p \geq 1 \tag{28}$$

Thus it will always be on the conservative side to assume $S_p = 1.0$.

In the case of debonds, it may be appropriate to treat the damage as level 1 and use the local factor R_l, but in some cases the debond size may be too large for this and have to be treated as level 2, or even level 3 damage.

Any panel that experiences damage should be checked by comparing R_p with a minimum allowable value R_{pa}:

$$R_p \geq R_{pa} \text{ where } R_p = \min(R_l S_p, 1) \tag{29}$$

R_{pa} represents the minimum residual load-carrying capacity that can be allowed for the panel concerned, based on consideration of maintaining the panel's functionality. Such a limit can be defined for either local or global loading cases, or both.

If the damaged panel contributes to the global strength of the ship, as, for example, with a hull bottom panel amidships, the overall consequences for the ship must also be assessed. For this purpose the ship strength reduction factor R_s is estimated for one or more global loading cases. For level 1 and 2 damage types, this can be done using a panel location and load type factor S_s that is analogous to the local location and load type sensitivity factor S_p so that

$$R_s = R_p S_s \text{ with a maximum value of 1.0.} \tag{30}$$

The factor S_s represents the reserve of strength at the panel in which the damage occurs, calculated for the intact condition. Overall analysis of the intact ship can be used to establish a map showing reserves of strength in its respective panels, and an S_s value attached to each panel.

For level 3 damage, an approximate method has been proposed [5] for estimating R_s based on assumptions about the reduction of panel stiffness induced by the damage. If this is not appropriate, and for level 4 damage, a direct assessment of the damaged ship must be performed.

Finally the ship strength reduction R_s has to be compared with an allowable value R_{sa} based on evaluation of the required margin of safety for the design of the ship as a whole.

$$R_s \geq R_{sa} \text{ where } R_s = \min(R_p S_s, 1) \tag{31}$$

The total assessment process is illustrated in Fig. 20.

The global strength criterion can be checked directly, but experience has shown that it may be more convenient to transform it to either the panel or the local level, so that R_{sa} is used to establish an allowable panel strength reduction factor R_{paG} and, where appropriate, an allowable local strength reduction factor R_{laG} for global loads. This will ensure that the values of R_p and R_l will not lead to violation of the global
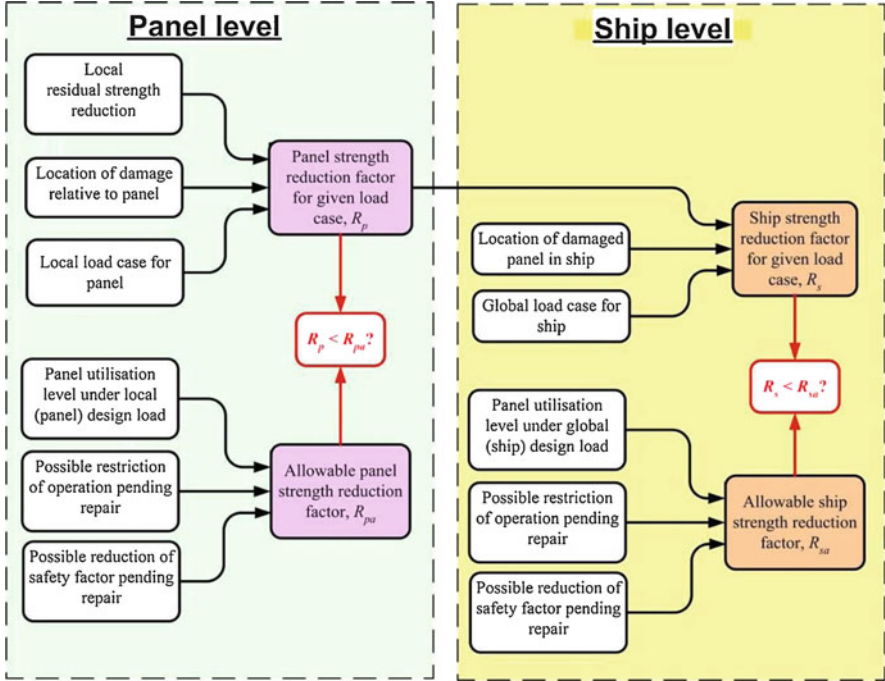
Fig. 20 Schematic diagram illustrating the strength assessment process in the presence of damage

ship strength reduction criterion. From Eqs. 27, 28, 29, 30 and 31 it can be shown that

$$R_{paG} = \min\left(\frac{R_{sa}}{S_s}, \frac{1}{S_s}\right) \quad \text{and} \quad R_{laG} = \min\left(\frac{R_{sa}}{S_pS_s}, \frac{1}{S_pS_s}\right) \tag{32}$$

Then the condition $R_s \geq R_{sa}$ can be applied at either the panel or the local level:

$$R_p \geq R_{paG} = \min\left(\frac{R_{sa}}{S_s}, \frac{1}{S_s}\right) \quad \text{or} \quad R_l \geq R_{laG} = \min\left(\frac{R_{sa}}{S_pS_s}, \frac{1}{S_pS_s}\right) \tag{33}$$

Since normally $R_{sa} \leq 1$ these criteria normally reduce to

$$R_p \geq R_{paG} = \frac{1}{S_s} \quad \text{or} \quad R_l \geq R_{laG} = \frac{1}{S_pS_s} \tag{34}$$

Application at the panel level is often most convenient. However, the formulation at the local level is relevant for the extension to damage growth under cyclic loading (see Sect. 5.5). The allowable strength reduction factors for local load cases are

designated R_{paL} and R_{laL}, and those for global load cases R_{paG} and R_{laG}. By similar arguments to the above,

$$R_{laL} = \min\left(\frac{R_{paL}}{S_p}, \frac{1}{S_p}\right) \tag{35}$$

Apart from establishment of the strength reduction at the lowest level, all the factors required can be obtained from prior analysis of the intact ship and its components, considering the relevant loading conditions on the ship in service. If this is properly planned during the design process, it can be performed as part of the design calculations with only modest extra effort.

Note also that the simple relationships between the local, panel and ship scales for level 1 and 2 damage cases are made possible by the assumption that small cases of damage do not significantly influence the panel stiffness, so that the loading distribution between different parts of the structure are not significantly affected by the damage.

Once the checks against the acceptable strength reductions at the appropriate scales have been performed, a decision can be made on further actions bearing in mind the situation in which the vessel is operating. The options may include (in roughly ascending order of severity:

- No repair, no action
- No immediate repair:

  – Maintain operational profile and

    o Monitor damage, decide on repair later
    o Repair at next scheduled docking (with or without monitoring of damage)
    o Proceed to safe harbour and repair there (or make new assessment)
    o Proceed to dry dock and repair there

  – Change operational profile and repair later (same options as above)

- Immediate repair at sea

  – Permanent repair, retain operational profile
  – Emergency/temporary repair. Options then as for "No immediate repair"

- Abandon ship

5.4 Simplified Procedure Developed for On-Board Use

In connection with the development of on-board inspection and repair manuals for a specific series of naval vessels, a simplified procedure was developed for level 1 type damage that used a classification system to represent the damage severity and the load and location factors. Level 1 damage is divided into five severity classes

1A to 1E according to their R_l values. For use in the panel assessment for local load cases, a series of SPL categories is similarly defined according to values of S_{pL}. A panel strength reduction category RPL0 to RPL5 can then be found from a simple table for any given combination of damage level (1A-1E) and SPL category.

The RPL categories are defined in accordance with minimum values of the factor R_{pL}. In a similar way, a set of categories for minimum allowable panel strength reduction factor is defined.

For each type of damage (e.g. sharp or blunt impact, debond) a basic data sheet is provided that includes how to identify and measure the damage and place it in the correct level.

The damage assessment is applied at the panel scale for both local and global load cases. Each panel on the ship (or a group of similar panels) is provided with a data sheet that indicates its main functions and type of loading, and, together with the damage data sheet, provides all the necessary data and categories for use in the damage assessment. Numerical values of the various factors are provided in addition to category codes.

5.5 Application to Fatigue Loading

Hayman and Berggreen [77] recently proposed a way in which the SaNDI approach might be extended to cover fatigue loading. With cyclic loading on level 1 damage, the local strength reduction curve should in principle be replaced by a residual life reduction curve. However, this would have to be drawn for a given load level (as amplitude of load cycles) and given minimum/maximum load or stress ratio. As the damage shape is likely to change during crack growth, it is most appropriate to use the minimum/maximum ratio for the far-field stress. Figure 21 shows schematically a set of such curves. Unlike the residual strength curves for static loading, these curves intersect with the horizontal axis at the points representing the condition

Fig. 21 Residual life reduction curves (schematic)
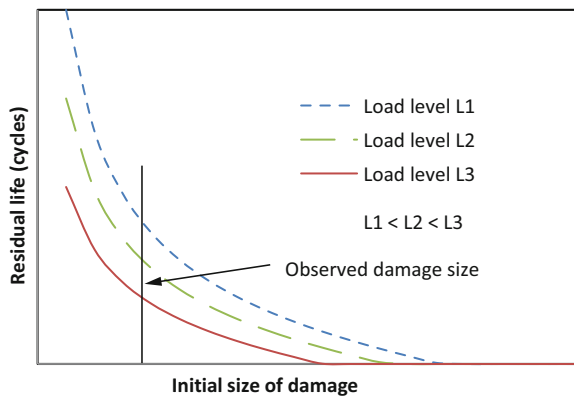
where the applied maximum load is equal to the residual strength of the component in its initial damaged state.

How to define the residual life can only be decided when some experience has been acquired regarding the way in which the damage growth occurs for the particular type of damage. It seems likely that the rate of growth will accelerate as the residual strength is reduced toward the level of the applied loading cycles.

For a given observed damage size and load amplitude, it is possible to read off the expected residual life. This can be compared with the minimum acceptable residual life and a decision made on further actions bearing in mind the situation in which the vessel is operating. The options will be similar to those listed in Sect. 5.3, but now the decision can be based on an estimate of the time it will take before the damage becomes critical.

A weakness of the above description is that it assumes that the load level is known. This information may be available for the scenario in question, but if it is not it is still possible to use R_{laG} given by Eq. (32), or the value of R_{laL} given by Eq. (35), to give a maximum allowable load value. This maximum allowable load is given by multiplying the intact static strength by R_{laG} or R_{laL}. As load values above this would violate the static strength acceptance criterion, this must give a conservative estimate for the residual fatigue life.

A further weakness lies in the fact that, although the initial damage may be small enough to class it as level 1, growth under cyclic loading might possibly increase the size beyond level 1. However, if the same type of damage has been considered under static loading and found to give failure while the size is within level 1, it is unlikely this will be a problem, though change of shape of the damage during growth might of course invalidate this assumption. Such situations will, however, become clear during the analysis or testing at the local scale.

Another approach is to use the same data as presented in Fig. 21 but plot the load level (amplitude) against the initial size of damage, for a series of values of residual life. In such a plot the load level can be made dimensionless by dividing it by the intact strength, as shown schematically in Fig. 22. This is the inverse of what is normally calculated, because the residual life would be calculated based on a given

Fig. 22 Strength reduction curves for different numbers of fatigue cycles (schematic)
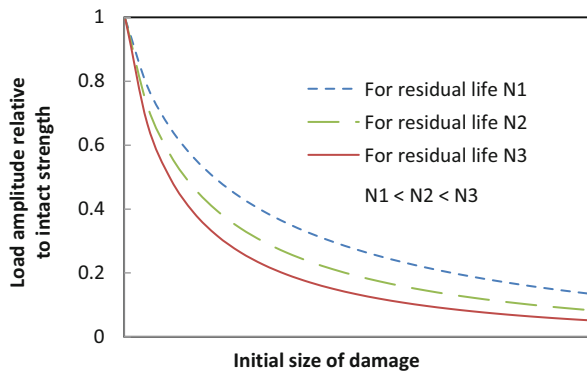
load amplitude. The required inversion process would necessarily involve interpolation between actual calculated cases. A major advantage of this approach is that the SaNDI damage assessment procedure can be applied directly, with use of the load type and location factors as for static loading. In effect we now have a series of local strength reduction curves for given desired values of residual life. For level 2 damage types, similar curves can be drawn at the panel level.

5.6 Direct Estimation of Residual Fatigue Life: Integrated Fatigue Prediction System

The generation of residual fatigue life curves of the type described in Sect. 5.5 is an extremely demanding task. An alternative to this approach is to provide a tool that will allow direct estimation of the residual life for a specific debond damage case when detected. Such a tool has long been sought after by the aircraft industry. A significant step towards the establishment of such a tool was recently reported by Farshidi et al. [78]. The system consists of a series of scripts for use with the ABAQUS software system, and is largely based on the principles for predicting fatigue life of debonded sandwich panels described earlier in this chapter. However, it has so far only been applied to a typical aircraft structural component and loading, namely a sandwich panel with honeycomb core, subjected to ground-air-ground (GAG) load cycles giving defined cyclic pressure changes inside the core. This can in principle be applied to naval sandwich structures by replacing the honeycomb with an appropriate foam core and implementing an appropriate loading. However, an appropriate, representative fatigue loading for a naval vessel will have to be defined: for a sandwich hull or deck panel it might result from local loads giving lateral pressure on the panel or global hull loads giving mainly in-plane tension or compression, or a combination of these. Note that such a tool could also be used for parametric studies to pre-calculate residual life curves as described in Sect. 5.5.

6 Conclusion

Modelling and physical testing of sandwich structures with face-core debonds at both the small, characterisation test specimen scale and the larger, ship structural component scale, have progressed considerably during the past few decades. Knowledge gained from such research is essential for the systematic implementation of damage tolerance principles in the design and operation of naval ships employing FRP sandwich construction. Much of the underlying research in recent years has been carried out at the Technical University of Denmark and at collaborating universities and research institutions. A significant amount of this research has been supported by the ONR's Solid Mechanics Research Program. This chapter

has attempted to provide an overview of this research, and especially the progress made during the past 10–15 years. Previously developed schemes for assessing damage experienced by sandwich structures in naval ships and their influence on residual structural strength have been described and discussed. Possibilities for devising similar procedures for assessing residual fatigue life following a damage event have been explored.

References

1. Hayman B (2003) Inspection and repair of sandwich structures based on damage tolerance principles. In: Vinson JR, Rajapakse YDS, Carlsson LA (eds) 6th International Conference on Sandwich Structures. CRC Press, Boca Raton, pp 955–963
2. Hayman B, Zenkert D (2004) The influence of defects and damage on the strength of FRP sandwich panels for naval ships. In: Keil H, Lehmann E (eds) 9th International Symposium on Practical Design of Ships and Other Floating Structures (PRADS 2004). Seehafen Verlag GmbH, Hamburg, pp 719–726
3. Hayman B (2004) Defect and damage assessment for ships built in FRP sandwich. In: RINA Conference on High Speed Craft, Royal Institution of Naval Architects, London, November 2004
4. Zenkert D, Shipsha A, Bull P et al (2005) Damage tolerance assessment of composite sandwich panels with localised damage. Compos Sci Technol 65(15–16):2597–2611
5. Hayman B (2007) Approaches to damage assessment and damage tolerance for FRP sandwich structures. J Sandw Struct Mater 9(6):571–596
6. Berggreen C (2004) Damage tolerance of debonded sandwich structures, Ph.D. Thesis, Department of Mechanial Engineering, Technical University of Denmark
7. Zenkert D (1991) Strength of sandwich beams with interface debondings. Compos Struct 17:331–350
8. Zenkert D (1990) Damage tolerance of foam core sandwich constructions. Doctoral thesis published as Report No. 90–8, Royal Institute of Technology (KTH), Stockholm, Sweden 1990
9. Carlsson LA, Kardomateas GA (2011) Structural and failure mechanics of sandwich composites. Springer, Netherlands
10. Griffith AA (1921) The phenomena of rupture and flow in solids. Philos Trans R Soc Lond 221:163–198
11. Suo Z (1990) Singularities, interfaces and cracks in dissimilar media. Proc R Soc Lond A 427:331–358
12. Suo Z, Hutchinson JW (1990) Interface crack between two elastic layers. Int J Fract 43(1):1–18
13. Dundurs J (1969) Discussion on "Edge-bonded dissimilar orthogonal elastic wedges under normal and shear loading". J Appl Mech 36:650–652
14. Hutchinson JW, Suo Z (1991) Mixed mode cracking in layered materials. Adv Appl Mech 29:63–191
15. Suo Z (1989) Singularities interacting with interfaces and cracks. Int J Solids Struct 25 (10):1133–1142
16. Prasad S, Carlsson LA (1994) Debonding and crack kinking in foam core sandwich beams – I: Analysis of fracture specimens. Eng Fract Mech 47:813–824

17. Prasad S, Carlsson LA (1994) Debonding and crack kinking in foam core sandwich beam – II: Experimental investigation. Eng Fract Mech 47:825–841
18. Rice JR (1968) A path-independent integral and the approximate analysis of strain concentration by notches and cracks. J Appl Mech 35:376–386
19. Berggreen C, Simonsen BC (2005) Non-uniform compressive strength of debonded sandwich panels - II. Fracture mechanics investigation. J Sandw Struct Mater 7(6):483–517
20. Berggreen C, Simonsen BC, Borum KK (2007) Experimental and numerical study of interface crack propagation in foam cored sandwich beams. J Compos Mater 41(4):493–520
21. Rybicki EF, Kanninen MF (1977) A finite element calculation of stress intensity factors by a modified crack closure integral. Eng Fract Mech 9(4):931–938
22. Raju IS (1987) Calculation of strain-energy release rates with higher order and singular finite elements. Eng Fract Mech 28(3):251–274
23. Williams M (1959) The stresses around a fault or crack in dissimilar media. Bull Seismol Soc Am 49(2):199–204
24. Erdogan F (1963) Stress distribution in a nonhomogeneous elastic plane with cracks. J Appl Mech 30(2):232–236
25. Paris P, Erdogan F (1963) A critical analysis of crack propagation laws. J Basic Eng 85(4):528–534
26. Moslemian R, Karlsson AM, Berggreen C (2011) Accelerated fatigue crack growth simulation in a bimaterial interface. Int J Fatigue 33(12):1526–1532
27. Moslemian R, Berggreen C, Karlsson AM (2012) Face/core debond propagation in sandwich panels under cyclic loading - Part I: Numerical modeling. In: 10th International Conference on Sandwich Structures. Nantes, France, pp 41–42
28. Moslemian R, Berggreen C, Karlsson AM (2012) Face/core debond propagation in sandwich panels under cyclic loading - Part II: Experimental validation. In: 10th International Conference on Sandwich Structures. Nantes, France, pp 43–44
29. ASTM standard C393–62 Standard method of flexure test of flat sandwich constructions. American Society for Testing and Materials, Philadelphia
30. Carlsson LA, Sendlein LS, Merry SL (1991) Characterization of face sheet/core shear fracture of composite sandwich beams. J Compos Mater 25:101–116
31. Carlsson LA (1991) On the design of the cracked sandwich beam (CSB) specimen. J Reinf Plast Compos 10:434–444
32. ASTM C273-61 (1991) Shear test in flatwise plane of flat sandwich construction and sandwich cores. American Society for Testing and Materials, Philadelphia
33. Carlsson LA, Matteson RC, Aviles F, Loup DC (2005) Crack path in foam cored DCB sandwich fracture specimens. Compos Sci Technol 65:2612–2621
34. Aviles F, Carlsson LA (2007) Analysis of the sandwich DCB specimen for debond characterization. Eng Fract Mech 75:153–168
35. Sørensen BF, Jørgensen K, Jacobsen TK, Østergaard RC (2006) DCB-specimen loaded with uneven bending moments. Int J Fract 141:163–176
36. Lundsgaard-Larsen C, Sørensen BF, Berggreen C, Østergaard RC (2008) A modified DCB sandwich specimen for measuring mixed mode cohesive laws. Eng Fract Mech 75(8):2514–2530
37. Kardomateas GA, Berggreen C, Carlsson LA (2013) Energy release rate and mode mixity of a face/core debond in a sandwich beam. AIAA J 51(4):885–892. https://doi.org/10.2514/1.J051765
38. Saseendran V, Berggreen C, Carlsson LA (2018) Fracture mechanics analysis of reinforced DCB sandwich debond specimen loaded by moments. AIAA J 56(1):413–422. https://doi.org/10.2514/1.J056039
39. Berggreen C, Saseendran V, Carlsson LA (2018) A modified DCB-UBM test method for interfacial fracture toughness characterization of sandwich composites. Eng Fract Mech 203:208–223. https://doi.org/10.1016/j.engfracmech.2018.06.036

40. Li X, Carlsson LA (1999) The tilted sandwich debond (TSD) specimen for face/core interface fracture characterization. J Sandw Struct Mater 1(1):60–75
41. Li X, Carlsson LA (2000) Elastic foundation analysis of tilted sandwich debond (TSD) specimen. J Sandw Struct Mater 2:3–32
42. Li X, Carlsson LA (2001) Fracture mechanics analysis of tilted sandwich debond (TSD) specimen. J Compos Mater 35:2145–2168
43. Viana GM, Carlsson LA (2002) Mode mixity and crack tip yield zones in TSD sandwich specimens with PVC foam core. J Sandw Struct Mater 4:141–155
44. Viana GM, Carlsson LA (2003) Influences of foam density and core thickness on debond toughness of sandwich specimens with PVC foam core. J Sandw Struct Mater 5:103–118
45. Berggreen C, Carlsson LA (2010) A modified TSD specimen for fracture toughness characterization – fracture mechanics analysis and design. J Compos Mater 44(15):1893–1912
46. Berggreen C, Quispitupa A, Costache A, Carlsson LA (2014) Face/core mixed mode debond fracture toughness characterization using the modified TSD test method. J Compos Mater 48 (16):1939–1945. https://doi.org/10.1177/0021998313492358
47. Quispitupa A, Berggreen C, Carlsson LA (2009) On the analysis of a mixed mode bending sandwich specimen for debond fracture characterization. Eng Fract Mech 76(4):594–613
48. Quispitupa A, Berggreen C, Carlsson LA (2010) Design analysis of the mixed mode bending sandwich specimen. J Sandw Struct Mater 12(2):253–272
49. Quispitupa A, Berggreen C, Carlsson LA (2011) Face/core interface fracture characterization of mixed mode bending sandwich specimens. Fatigue Fract Eng Mater Struct 34(11):839–853
50. Manca M, Quispitupa A, Berggreen C, Carlsson LA (2012) Face/core debond fatigue crack growth characterization using the sandwich mixed mode bending specimen. Compos Part A 43:2120–2127
51. Manca M, Berggreen C, Carlsson LA (2015) G-control fatigue testing for cyclic crack propagation in composite structures. Eng Fract Mech 149:375–386. https://doi.org/10.1016/j.engfracmech.2015.06.059
52. Manca M, Berggreen C, Carlsson LA, Bortolotti P (2016) Fatigue characterization of poly vinyl chloride (PVC) foam core sandwich composite using the G-control method. J Sandw Struct Mater 18(3):374–394. https://doi.org/10.1177/1099636215603049
53. Sabbadin P, Berggreen C, Nygard B (2018) Development of a mode I/II/III test fixture for composite laminates and sandwich face/core fracture characterization. In: 12th International Conference on Sandwich Structures, Lausanne, Switzerland, pp 35–37
54. Davidson BD, Sediles FO (2011) Mixed-mode I-II-III delamination toughness determination via a shear-torsion-bending test. Compos Part A 42:589–603
55. Barbieri L, Massabo R, Berggreen C (2018) The effects of shear and near tip deformations on interface fracture of symmetric sandwich beams. Eng Fract Mech 201:298–321. https://doi.org/10.1016/j.engfracmech.2018.06.039
56. Farshidi A, Berggreen C, Carlsson LA (2019) Low temperature mixed-mode debond fracture and fatigue characterisation of foam core sandwich. J Sandwich Struct Mater in press:109963621877942. https://doi.org/10.1177/1099636218779420
57. Layne AM, Carlsson LA (2002) Test method for measuring strength of a curved sandwich beam. Exp Mech 42:194–199
58. Layne AM, Carlsson LA (2002) Flexural strength of curved sandwich beams with face/core debond. J Sandw Struct Mater 4:203–217
59. Aviles F, Carlsson LA (2005) Elastic foundation analysis of local face buckling in debonded sandwich columns. Mech Mater 37:1026–1034
60. Moslemian R, Berggreen C, Carlsson LA, Avilés F (2009) Failure investigation of debonded sandwich columns: an experimental and numerical study. J Mech Mater Struct 4 (7–8):1469–1487
61. Nøkkentved A, Lundsgaard-Larsen C, Berggreen C (2005) Non-uniform compressive strength of debonded sandwich panels – I. Experimental investigation. J Sandw Struct Mater 7 (6):461–448

62. Moslemian R, Quispitupa A, Berggreen C, Hayman B (2012) Failure of uniformly compression loaded debond damagedsandwich panels - an experimental and numerical study. J Sandw Struct Mater 14(3):297–324
63. Aviles F, Carlsson LA (2006) Experimental study of debonded sandwich panels loaded in compression. J Sandw Struct Mater 8:7–30
64. Aviles F, Carlsson LA (2005) Face sheet buckling of debonded sandwich panels using a 2D elastic foundation approach. Mech Adv Mater Struct 12(5):349–361
65. Aviles F, Carlsson LA (2006) Three-dimensional finite element buckling analysis of debonded sandwich panels. J Compos Mater 40(11):993–1008
66. Aviles F, Carlsson LA (2007) Post-buckling and debond propagation in sandwich panels subject to in-plane loading. Eng Fract Mech 74:794–806
67. Jolma P, Segercrantz S, Berggreen C (2007) Ultimate failure of debond damaged sandwich panels loaded with lateral pressure – an experimental and fracture mechanical study. J Sandw Struct Mater 9(2):167–196
68. Moslemian R, Berggreen C (2013) Interface fatigue crack propagation in sandwich X-joints – Part I: Experiments. J Sandw Struct Mater 15(4):1–22
69. Moslemian R, Berggreen C (2013) Interface fatigue crack propagation in sandwich X-joints – Part II: Finite element modeling. J Sandw Struct Mater 15(4):23–36
70. Lundsgaard-Larsen C, Berggreen C, Carlsson LA (2010) Tailoring sandwich face/core interfaces for improved damage tolerance - Part I: Finite element analysis. Appl Compos Mater 17 (6):609–619
71. Lundsgaard-Larsen C, Berggreen C, Carlsson LA (2010) Tailoring sandwich face/core interfaces for improved damage tolerance - Part II: Experiments. Appl Compos Mater 17 (6):621–637
72. Martakos G, Andreasen JH, Berggreen C, Thomsen OT (2017) Interfacial crack arrest in sandwich panels with embedded crack stoppers subjected to fatigue loading. Appl Compos Mater 24:55–76. https://doi.org/10.1007/s10443-016-9514-3
73. Martakos G, Andreasen JH, Berggreen C, Thomsen OT (2019) Experimental investigation of interfacial crack arrest in sandwich beams subjected to fatigue loading using a novel crack arresting device. J Sandw Struct Mater 21(2):401–421. https://doi.org/10.1177/1099636217695057
74. Martakos G, Andreasen JH, Berggreen C, Thomsen OT (2019) Interfacial crack arrest in sandwich beams subjected to fatigue loading using a novel crack arresting device - numerical modelling. J Sandw Struct Mater 21(2):422–438. https://doi.org/10.1177/1099636217695058
75. Hayman B, Berggreen C, Petterson R (2007) Tests and analyses of FRP sandwich structures with face sheet wrinkles. J Sandw Struct Mater 9(4):377–404
76. Hayman B, Echtermeyer AT (2019) Reduction of strength of GFRP sandwich panels in naval ships by face sheet holes, cracks and impact damage. J Sandw Struct Mater 21:1621–1653. https://doi.org/10.1177/1099636219836357
77. Hayman B, Berggreen C (2018) Damage assessment schemes for naval sandwich structures with face-core debonds considering residual strength and fatigue life. In: 12th International Conference on Sandwich Structures, Lausanne, Switzerland, pp 32–34
78. Farshidi A, Berggreen C (2019) Analysis of disbonded aircraft sandwich panels with unvented honeycomb cores. Compos Part B, submitted 2019